Computers, Environment and Urban Systems 127 (2026) 102438

Contents lists available at ScienceDirect

Computers, Environment and Urban Systems

journal homepage: www.elsevier.com/locate/ceus

A tree location optimization via metamodel-based simulation framework for mitigating extreme heat in communities

Yuhong Bai, Wangshu Mu *, Changqing Song

Faculty of Geographical Science, Beijing Normal University, China

ARTICLE INFO

Keywords:
Cooling effect of trees
Swin-Unet
Genetic algorithm
Tree spatial distribution

ABSTRACT

The exacerbation of the urban heat island effect, driven by rapid urbanization, necessitates effective thermal mitigation strategies. While urban forestry presents a cost-effective solution for improving the thermal environment, optimizing tree placement to maximize cooling benefits remains a significant computational challenge. Conventional optimization methods rely on iterative calls to physics-based climate models, a process so computationally intensive that it often forces compromises in spatial resolution and model fidelity. This study overcomes this limitation by proposing a novel framework, namely, the Swin-Unet Guided Multiscale Hybrid Genetic Algorithm (SU-MHGA), that couples a deep learning model with a multiscale hybrid genetic algorithm. We employ the Swin-Unet architecture to serve as a rapid and accurate metamodel, capable of predicting the mean radiant temperature (T_{mrt}) distribution for any given tree configuration. This predictive model is then integrated into an optimization workflow driven by a genetic algorithm and refined with local enumeration to efficiently search for the optimal spatial arrangement of trees. The objective is to identify the tree distribution plan that maximizes the reduction in T_{mrt}. Comparative analysis demonstrates that the optimized tree layouts generated by SU-MHGA achieve a more significant reduction in T_{mrt} than those produced by the benchmark TreePlanter software, while also requiring substantially less computational time. Specifically, SU-MHGA achieved a 17-fold acceleration in T_{mrt} prediction compared to the SOLWEIG model; and demonstrated up to a 135-fold improvement in optimization speed when planting 15 trees compared to TreePlanter. This research effectively bridges the gap between high-fidelity microclimate simulation and applied urban planning, making strategic thermal mitigation accessible for real-world implementation.

1. Introduction

As cities expand and temperatures rise due to climate change, extreme heat is becoming a critical challenge for urban communities, especially in neighborhoods with limited greenery and high-density development (Abunnasr et al., 2022). This extreme heat severely impacts on the quality of life for urban residents, increasing heat-related illnesses, energy demands, and mortality rates (Diallo et al., 2024; Kearl & Vogel, 2023), particularly in vulnerable communities (Chen & He, 2024). Strategically planted trees offer a powerful, community-centered solution (Keenan et al., 2025). By providing shade and releasing moisture through transpiration, trees significantly lower local temperatures and improve livability in neighborhood (Tan et al., 2017; Wang, Zhou, & Jiao, 2022). Beyond temperature regulation, trees enhance community well-being by improving air quality, reducing noise pollution, and fostering social interaction in parks and green corridors (Grote et al., 2016; Lu et al., 2024).

The spatial distribution of trees critically determines their cooling efficacy, as suboptimal arrangements can diminish thermal benefits across multiple dimensions. Studies employing canopy radiation transfer models demonstrate that excessive planting densities lead to canopy overlap, which creates redundant shading in already protected areas and consequent resource inefficiencies (Wang et al., 2021). Furthermore, dense canopy cover can impede nocturnal longwave radiative heat loss from surface and lower atmospheric layers, thereby attenuating diurnal cooling (Froelich et al., 2011). Conversely, overly sparse distributions generate discontinuous shade, failing to mitigate temperatures effectively in critical 'hotspot' zones (Elkhateeb & Anwar, 2025). The microscale placement of individual trees also plays a pivotal role; trees situated in existing shade contribute significantly less to temperature reduction than those positioned in sunlit areas, as they do not actively intercept direct solar radiation (Wu et al., 2019).

* Corresponding author.
E-mail address: muwangshu@bnu.edu.cn (W. Mu).

https://doi.org/10.1016/j.compenvurbsys.2026.102438
Received 28 October 2025; Received in revised form 25 March 2026; Accepted 2 April 2026
Available online 15 April 2026

However, identifying optimal planting locations to maximize this benefit remains a complex challenge. Current microclimate simulation models, such as SOLWEIG, involve intricate calculations to simulate interactions between buildings, trees, and neighborhood environment (Xu et al., 2025). Spatial optimization of tree placement typically requires repeatedly running these simulations to evaluate how different planting configurations affect local temperatures, which is a computationally demanding process. As a result, simplified spatial optimization models are often employed, leading to compromised solutions in spatial resolution and optimality (Hosseinzadeh & Keshmiri, 2021; Xu et al., 2025).

To address the challenge of optimizing urban tree spatial distribution, we propose an innovative optimization via metamodel-based simulation framework, namely the Swin-Unet Guided Multiscale Hybrid Genetic Algorithm (SU-MHGA), which combines deep learning with spatial optimization. Compared to conventional urban tree optimization models, SU-MHGA introduces the following methodological innovations: We replace computationally intensive microclimate simulations with a pre-trained deep learning metamodel surrogate, which sacrifices minimal accuracy while dramatically improving computational performance. This metamodel facilitates efficient optimization using a multiscale hybrid genetic algorithm (GA). By first conducting a global search via GA, then refining solutions through localized enumeration, SU-MHGA enables a more comprehensive exploration of possible tree distributions than existing methods.

The paper is organized as follows: First, the Background section reviews recent advances in tree radiation simulation and spatial optimization models. Next, the Methods section introduces the problem formulation and solution approach. We then validate the model's effectiveness and computational efficiency using a real-world case study from Tucson, USA. Finally, based on the test results, we discuss key insights and present conclusions.

2. Background

2.1. Microclimate effect of trees at the community scale

Urban greening, particularly tree planting, is a key strategy for mitigating extreme heat and its associated health risks in cities (Bowler et al., 2010). Community-scale greening initiatives have gained increasing attention due to their practical and innovative potential (Bosch et al., 2021). Small urban green spaces—such as pocket parks, community gardens, and street trees—play a disproportionately large role in urban ecosystems, delivering critical ecosystem services despite their limited size (Dennis & James, 2016; Strohbach et al., 2013). Vegetation, especially trees, regulates outdoor microclimates through multiple mechanisms: transpiration cools ambient temperatures (Meili et al., 2021), while shading reduces direct solar radiation (Wu et al., 2023). However, trees may also impede airflow (Zheng et al., 2023) and elevate humidity (Gao et al., 2025), occasionally generating unintended microclimatic trade-offs. Thus, strategic greening design is essential for optimal microclimate regulation.

At the community level, urban greening research holds particular significance. In contrast to macro-scale citywide planning, small-scale interventions emphasize precision management and participatory governance, ensuring alignment with local residential needs (Keenan et al., 2025). Optimizing tree spatial distribution in urban neighborhoods not only enhances ecological benefits but also strengthens community resilience and livability. Existing studies have shown that there are differences in the mean radiant temperature between regular grid pattern planting and staggered alternating planting. This is primarily due to the impact of tree alignment—whether perpendicular or parallel to the prevailing wind direction—on ventilation efficiency and evaporative cooling effects (Abdi et al., 2020). Additionally, trees exhibit strong ecological resilience even under extreme high-temperature conditions. Research has found that deciduous species such as ash trees demonstrate enhanced cooling functions during summer heatwaves and droughts (Schneider et al., 2021).

While trees influence the thermal environment through multiple pathways, their most direct impact on human thermal comfort comes from radiation reduction (Du et al., 2020; Zhang, Spence, et al., 2022). This effect can be quantitatively measured using the mean radiant temperature (T_{mrt}), which integrates all longwave and shortwave radiant fluxes absorbed by the human body (Mayer et al., 2009; Mayer & Höppe, 1987). It serves as a key indicator for assessing thermal comfort (Chen et al., 2008), with higher values signaling potential heat-related health risks (Zhao et al., 2018). Notably, during extreme heat events, elevated T_{mrt} correlates strongly with increased mortality (Thorsson et al., 2014).

Empirical research demonstrates that urban trees significantly lower T_{mrt}, enhancing livability. For example: In Tanzania's tropical humid climate, trees reduce midday T_{mrt} by 7.9–12.2 °C (Baruti et al., 2024). In subtropical monsoon regions like Hong Kong, dense canopies lower T_{mrt} by up to 5.1 °C compared to open spaces (Kong et al., 2017). In tropical Singapore, tree planting in exposed areas reduces peak T_{mrt} by 14–25 °C (Tan et al., 2013). These findings underscore trees' critical role in mitigating urban heat stress through radiative cooling.

2.2. Simulation of urban tree cooling effects

Accurate simulation of trees' cooling effects is critical for optimizing their spatial distribution in urban areas. By modeling thermal performance, planners can identify tree arrangements that maximize cooling efficiency under resource and space constraints (Hao et al., 2023; Wang, Zhou, & Jiao, 2022). Empirical studies demonstrate that identical tree quantities planted in zones with high, moderate, and low solar radiation yield substantially different cooling outcomes (Wu & Chen, 2017). This variability is exacerbated by urban heterogeneity—where building morphology, material albedo, surface types, and existing vegetation create localized microclimates that unevenly distribute cooling benefits (Jiang et al., 2024; Zhang, Wang, et al., 2022). These complexities underscore the necessity of precision modeling, particularly at the community scale where microclimate interventions most directly impact livability.

The simulation of tree cooling effects primarily serves to quantify the dynamic interplay between vegetation and microclimatic regulation, providing critical insights for urban climate adaptation strategies. Widely used urban radiation models like SOLWEIG (Oswald et al., 2019) enable precise evaluation of thermal comfort and atmospheric conditions by simulating radiation fluxes and heat exchange processes in built environments, as conceptually illustrated in Fig. 1. These simulations reveal how each introduced tree modifies both shortwave and longwave radiation through two key mechanisms: (1) altered composite shading patterns resulting from tree-building interactions, and (2) modified reflection dynamics between vegetation elements and urban structures. Importantly, these changes manifest through the evolving interplay of direct shading effects and multi-reflective processes involving trees and buildings. The resultant transformations in local radiation budgets ultimately determine microclimate outcomes, highlighting why accurate simulation proves indispensable for evidence-based urban greening strategies - particularly in complex built environments where geometric configurations and material properties create highly nonlinear thermal responses.

In practical application, the SOLWEIG model necessitates two primary categories of input: meteorological forcing and three-dimensional spatial data. The spatial datasets determine the model's spatial granularity—as SOLWEIG operates without a fixed internal resolution—and typically comprise Digital Elevation Model(DSM), Digital Surface Model (DEM), Wall Height(WH) and Wall Aspect(WA), and optional surface cover classifications. Crucially, this spatial input incorporates the Sky View Factor (SVF), which the model calculates for both buildings and vegetation across 153 directions to derive an integral SVF value.

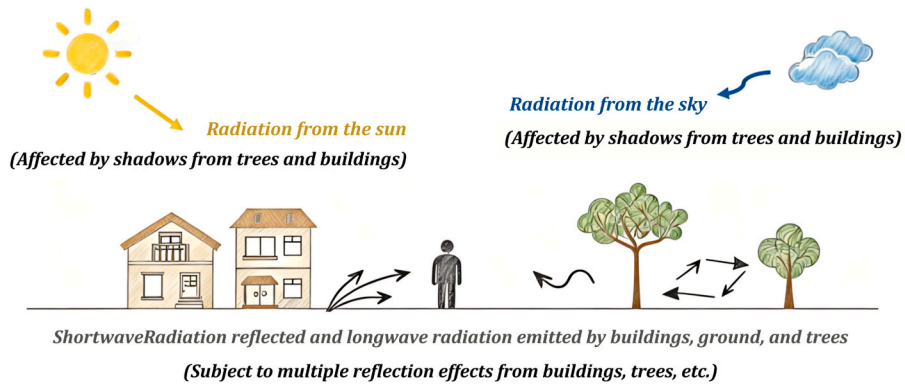

Fig. 1. Mechanism of SOLWEIG for calculating T_{mrt}.

Regarding meteorological inputs, the model requires only hourly, point-level data—specifically air temperature, relative humidity, wind speed, global solar radiation, and atmospheric emissivity. Consequently, SOLWEIG assumes a homogenous meteorological background where wind speed, humidity, and ambient temperature remain constant across the study area; this approach isolates urban morphology as the sole driver of spatial variations in the radiation field. By synthesizing these time-variant data, the model simulates the energy balance at every grid point to generate outputs such as upward and downward radiation fluxes, shadow patterns, and T_{mrt}. This structure allows researchers to accurately capture the dynamic effects of solar geometry and weather conditions on urban thermal comfort(Lindberg et al., 2008; Lindberg et al., 2018).

In addition to SOLWEIG, other widely-used urban radiation models include ENVI-met and RayMan (Matzarakis & Rutz, 2007). These models differ significantly in their scope and computational efficiency: ENVI-met provides comprehensive simulations of both longwave and shortwave radiation exchange on building surfaces, though its computational complexity restricts its application to small-scale studies. In contrast, RayMan excels at rapidly assessing human thermal radiation exposure but offers fewer output parameters, making it primarily suitable for single-point analyses. SOLWEIG strikes a balance between these approaches, demonstrating particularly strong utility for medium-to-large-scale simulations (Jänicke et al., 2021). This comparative analysis of model capabilities informs selection criteria based on research objectives, spatial scale, and required output parameters.

Quantifying the cooling effects of urban trees requires a multi-dimensional approach incorporating complementary modeling techniques. Computational Fluid Dynamics (CFD) simulations enable detailed analysis of airflow patterns and heat transfer processes through tree canopies (Toparlar et al., 2017), providing quantitative assessments of thermal comfort across different canopy configurations (An et al., 2025). Energy balance models offer another critical perspective by calculating latent heat fluxes from tree transpiration (Li et al., 2024), allowing researchers to estimate cooling effects under varying climatic conditions (Gkatsopoulos, 2017; Zheng et al., 2021). These approaches collectively demonstrate that accurate simulation of vegetative cooling necessitates the integration of multiple physical processes - including turbulent airflow, radiative transfer, and evapotranspiration - resulting in inherently complex computational challenges. The selection of modeling strategies should therefore align with specific research objectives while accounting for computational requirements.

2.3. Computational challenges in spatial optimization of urban trees

The spatial optimization of tree planting for thermal mitigation presents a significant computational challenge rooted in the complex dynamics of the urban microclimate (Hao et al., 2023; Wang, Li, et al., 2022). Unlike conventional paradigms such as the Maximum Coverage Location Problem (MCLP), which maximize static spatial coverage without accounting for physical processes (Church & ReVelle, 1974; Mu & Li, 2024), this problem requires explicitly modeling the mechanisms of heat transfer. The core difficulty lies in the highly nonlinear and tightly coupled nature of these thermal phenomena (Jaluria, 2009). These physical interactions defy simple algebraic parameterization, instead demanding sophisticated simulations to model effects such as the intricate thermal interplay between trees, sunlight, and buildings—a process that requires substantial computational resources (An et al., 2025).

Building upon quantitative studies of tree cooling effects and environmental benefits, researchers have increasingly explored spatial optimization algorithms for tree arrangement. Optimization efforts primarily utilize heuristic algorithms—including evolutionary algorithms (Stojakovic et al., 2020), greedy algorithms (Zhao et al., 2017), genetic algorithms (Ooka et al., 2008), and ant colony optimization (Shaamala & Yigitcanlar, 2024)—though these methods often face computational challenges, particularly slow convergence rates when applied to large-scale problems. The optimization objectives vary significantly depending on study area characteristics, commonly incorporating: (1) microclimate factors (solar radiation, temperature, shading, radiant load, and sky view factor); (2) human dimensions (thermal perception (Lusk et al., 2020) and equitable distribution (Nyelele & Kroll, 2021)); (3) environmental indicators (air pollution mitigation (Morani et al., 2011) and runoff regulation); and (4) economic considerations (planting costs (Ganjirad et al., 2025)). This multidimensional optimization framework reflects the complex trade-offs inherent in urban greening strategies.

To make the spatial optimization of tree planting computationally tractable, many models strike a balance between fidelity and efficiency by sacrificing accuracy or optimality. This is typically achieved by employing simple heuristic optimization algorithms or adopting coarse spatial resolutions. For instance, TreePlanter employs a hill-climbing algorithm to optimize tree placement using SOLWEIG-derived T_{mrt} and shadow grids alongside building data, bypassing the need for intensive, real-time physical modeling to reduce computational demands (Wallenberg et al., 2022). Similarly, Hao et al. (2023) accelerated climate simulations by partitioning their study area into coarse grids with uniform properties; this allowed them to compute only inter-partition energy flows rather than solve complex fluid differential equations pointwise, making the problem solvable with a genetic algorithm. Collectively, these approaches demonstrate a common strategy: achieving computational efficiency through spatial downsampling, aggregated inputs, or simplified physics.

2.4. Deep learning metamodels for efficient microclimate simulation

To mitigate the computational demands of microclimate simulations, researchers increasingly employ metamodels as efficient

approximations of high-fidelity simulators (Wu et al., 2021). As illustrated in Fig. 2, metamodels serve as low-cost proxies trained on limited simulation data to capture input-output relationships, enabling faster optimization (Lu & Ricciuto, 2019). For instance, Zhao et al. (2024) developed machine learning surrogates—Support Vector Regression (SVR) and Light Gradient Boosting Machine (LightGBM)—to predict local air temperature and wind speed efficiently, bypassing computationally intensive simulations during iterative design optimization. These models rapidly map design parameters (e.g., tree location, species) to outcomes (e.g., cooling effects), though their accuracy hinges on training data quality and model complexity (Hou & Behdinan, 2022).

Deep learning has revolutionized Earth system science by bypassing the need for manual feature engineering and complex physical modeling while still capturing complex Earth system dynamics, such as the radiative transfer process. Deep learning-based surrogate models instead learn input-output relationships from these simulations, enabling faster yet reliable approximations (Lagerquist et al., 2021; Stegmann et al., 2022). For instance, Huawei Cloud's Pangu Weather Model (Bi et al., 2023) uses Transformer architecture to accelerate meteorological predictions by 10,000 times, while Zhang et al. (2023) combine deep learning with physical laws to generate high-resolution forecasts in seconds, extending precipitation nowcasting to 3-h lead times. Given these advances in large-scale climate modeling, deep learning is poised to transform urban microclimate simulations as well.

Deep learning metamodels leverage neural networks to approximate input-output relationships from complex simulations or experimental data (Shlezinger et al., 2022). These surrogate models can replace computationally intensive simulations, facilitating the use of sophisticated optimization algorithms that would otherwise be impractical (Wang et al., 2025; Zani et al., 2024). For example, to improve SOLWEIG's computational efficiency, deep learning could potentially replace its entire radiation simulation process, significantly accelerating the mean radiant temperature predictions during tree arrangement optimization.

A key challenge in employing deep learning metamodels for urban climate simulation is the limited transferability or generalizability of trained models across different geographical locations (Baño-Medina et al., 2024). This limitation arises because these models are highly attuned to the specific statistical properties of the data on which they are trained. For instance, a model trained on data from a dense, high-rise urban core would not be directly applicable to a low-rise suburban area, as the underlying drivers of the microclimate—such as building geometry, material properties, and anthropogenic heat sources—differ significantly (Li et al., 2025; Xu et al., 2024). Consequently, implementing strategies to enhance model generalizability is imperative. Such approaches include sophisticated feature engineering to create location-agnostic inputs and the inclusion of training data from a wider geographical location to bridge the distributional gap between disparate urban contexts (Watson et al., 2022).

2.5. Innovations of this study

Notwithstanding substantial progress in microclimate simulation and tree layout optimization, critical methodological limitations persist. Primarily, the computational intractability of high-fidelity simulation models hinders their application in large-scale, iterative spatial optimization. Conversely, existing optimization strategies often compromise physical fidelity or spatial resolution to ensure computational feasibility, thereby sacrificing both prediction accuracy and global optimality. To address these challenges, this study proposes SU-MHGA, a novel coupled framework that integrates the Swin-Unet deep learning architecture—functioning as a high-efficiency radiation simulation surrogate—with a multi-scale hybrid genetic algorithm. This synergy delivers a significant enhancement in computational efficiency while preserving predictive rigor. By effectively resolving the conventional trade-off between computational cost and spatial precision, the framework enables a systematic search for globally optimal configurations, providing a robust, scientifically grounded strategy for community heat mitigation under extreme thermal conditions.

3. Study area

This study is situated in Tucson, Arizona, a city located in the southwestern United States characterized by a subtropical desert climate (Fig. 3). The region experiences abundant sunshine, intense solar radiation, and generally weak winds. Prolonged high temperatures are typical during summer months, with daily maximum temperatures ranging from 30 °C to 45 °C and frequent extreme heat events (Ghasemi Tousi et al., 2021). Given these conditions, the use of urban tree shade to mitigate outdoor radiant temperature is of particular importance in this area. The wind-ignoring radiation model SOLWEIG is well-suited for application in Tucson, as it effectively simulates both solar radiations received by ground surfaces and heat exchange processes within the urban environment.

4. Method

The workflow of this study is structured into two primary stages (also see Fig. 4): Metamodel Training and Tree Location Optimization. In Step 1 (Metamodel Training), LiDAR data is processed to generate key terrain variables (DEM, DSM, SVF, WH, WA). These are combined with randomly generated tree configurations (CDSM) and meteorological

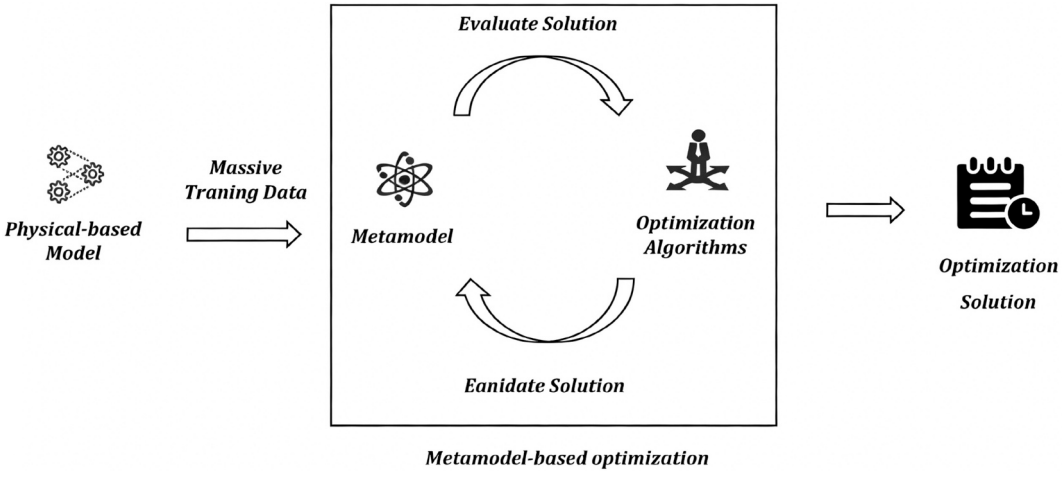

Fig. 2. Framework of metamodel-based optimization.

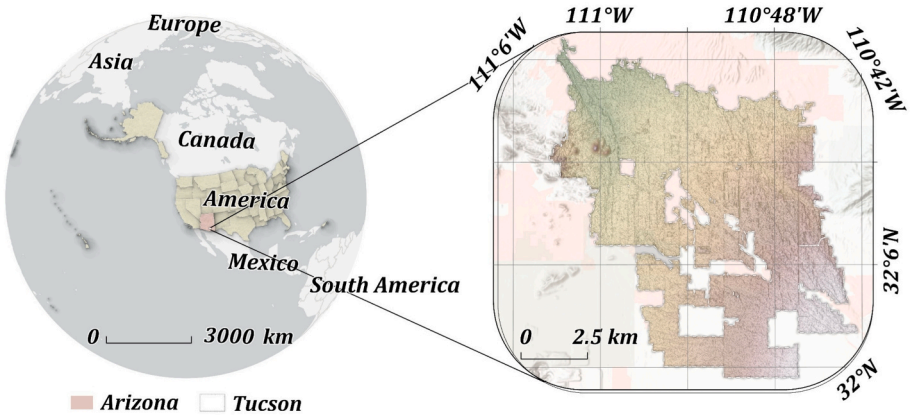

Fig. 3. Study area.

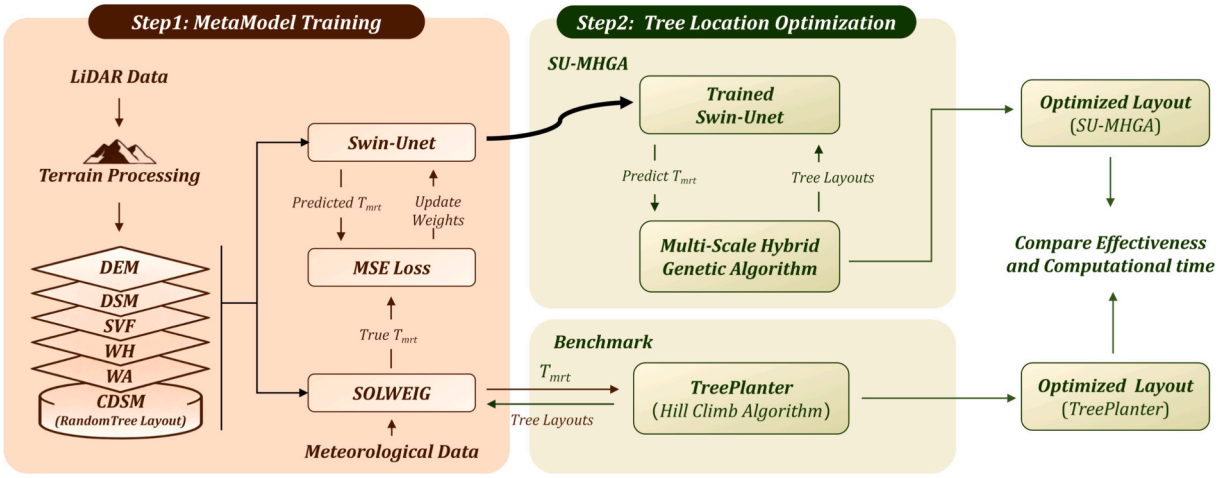

Fig. 4. Overall workflow of SU-MHGA.

data to compute ground-truth T_{mrt} using the SOLWEIG model. Concurrently, the six-channel geometric data serve as inputs for the Swin-Unet deep learning model. This network is iteratively trained to predict T_{mrt} by minimizing the Mean Squared Error (MSE) loss against the SOLWEIG-calculated benchmarks, yielding a robust surrogate model. Step 2 (Tree Location Optimization) integrates this trained Swin-Unet into a multi-scale hybrid genetic algorithm (SU-MHGA). The algorithm generates candidate planting layouts, which are rapidly evaluated by the surrogate model and refined through selection, mutation, and local enumeration operators to derive the optimal solution. To benchmark this approach, we compare it against TreePlanter, a hill-climbing optimization method that relies on direct SOLWEIG simulations for both identifying critical planting zones and evaluating iterative adjustments. The computational efficiency and cooling effectiveness of both algorithms are evaluated under identical boundary conditions to quantify their respective performance trade-offs.

4.1. Model specification

Let a rectangular study area be represented by a raster comprising w grids on the east-west axis and h grids on the north-south axis, for a total of $N = hw$ grid cells. The objective is to determine the optimal locations for planting k trees to minimize the daily mean T_{mrt}. Accordingly, the optimization model is formulated as follows:

Minimize:

$$\overline{T_{mrt}}(s) = \text{mean}(T_{mrt}(H_1, H_2, H_3(r,d,s), V_2, W_2, A_2)) \quad (1)$$

Subject to:

$$s = \{p^{(1)}, p^{(2)}, \ldots, p^{(k)}\} \subseteq S \quad (2)$$

$$S = \{(i,j)(i,j) \notin B, 1 \le i \le w, 1 \le j \le h\} \quad (3)$$

In this model, the decision variable s represents the locations of k trees, denoted as the set $\{p^{(1)}, p^{(2)}, \ldots, p^{(k)}\}$. These locations are selected from a set of permissible planting grids, S, which comprises all grid cells within the study area excluding a predefined set of forbidden locations, B, for example, those occupied by buildings. The objective function, as specified in Eq. (1), is to minimize the mean T_{mrt} across the study area (denote as $\overline{T_{mrt}}(s)$). This mean is calculated by averaging all N grid cell values in the $w \times h$ matrix T_{mrt}, which contains the daily mean radiant temperature for each grid.

The T_{mrt} matrix is derived from six parameters: the Digital Elevation Model (H_1), Digital Surface Model (H_2), Sky View Factor (V_2), Canopy Digital Surface Model ($H_3(r,d,s)$), wall aspect (A_2), and wall height (W_2). Crucially, only the Canopy Digital Surface Model, $H_3(r,d,s)$, is a function of the decision variable s. Two other parameters: canopy radius (r) and trunk height (d) also affect the Canopy Digital Surface Model. However, since we focus on how location of trees influence the cooling effect in community, we assume tree sizes are adjustable but will be predefined in the optimization process. The remaining five parameters H_1, H_2, S_2, W_2, and A_2 are treated as constants for a given study area but will vary if the study area changes.

The optimization objective is to minimize $\overline{T_{mrt}}(s)$. To overcome the significant computational expense of conventional simulation tools,

such as the SOLWEIG model, this research introduces a Swin-Unet model to predict T_{mrt}. The Swin-Unet is trained using six-channel input data: the Digital Elevation Model (DEM), Digital Surface Model (DSM), Canopy Digital Surface Model (CDSM), Sky View Factor (SVF), Wall Height (WH), and Wall Aspect(WA), with the corresponding T_{mrt} serving as the output.

The input channels utilized in SU-MHGA generally align with the standard SOLWEIG framework, with the primary distinction being the granularity of the SVF data. While SOLWEIG necessitates detailed obstruction metrics from 153 distinct directions, our model incorporates a single, aggregate SVF value. This dimensionality reduction was a deliberate design choice; due to the high correlation of obstruction values across adjacent directions, incorporating the full high-dimensional dataset would introduce significant multicollinearity, leading to unstable weight updates, gradient convergence difficulties, and potential overfitting. The aggregate SVF functions as a compressed representation, effectively retaining the essential spatial information required for the model. Furthermore, while SOLWEIG explicitly requires global parameters such as vegetation transmittance, building reflectivity, and emissivity, we excluded these from the input layer. In our deep learning architecture, these invariant physical properties are implicitly learned and encoded by the network, rendering explicit input redundant.

The high computational efficiency of this deep learning model is critical, as it enables the implementation of a sophisticated Multiscale Hybrid Genetic Algorithm for the optimization phase. This advanced algorithm is anticipated to yield superior results compared to simpler methods, such as the hill climbing algorithm, whose use is often necessitated by the prohibitive runtime of traditional physics-based models.

4.2. The Swin-Unet model for tree cooling effect simulation

4.2.1. Model construction

This study employs the Swin-Unet model to simulate T_{mrt}, serving as a computationally efficient alternative to conventional physics-based models. Swin-Unet is a deep learning architecture that integrates the hierarchical feature extraction of the Swin Transformer with the encoder-decoder structure of U-Net. This hybrid design is highly effective at capturing both global and local spatial information, making it well-suited for modeling complex, long-range dependencies (Tang et al., 2024). Although originally developed for pixel-wise classification in

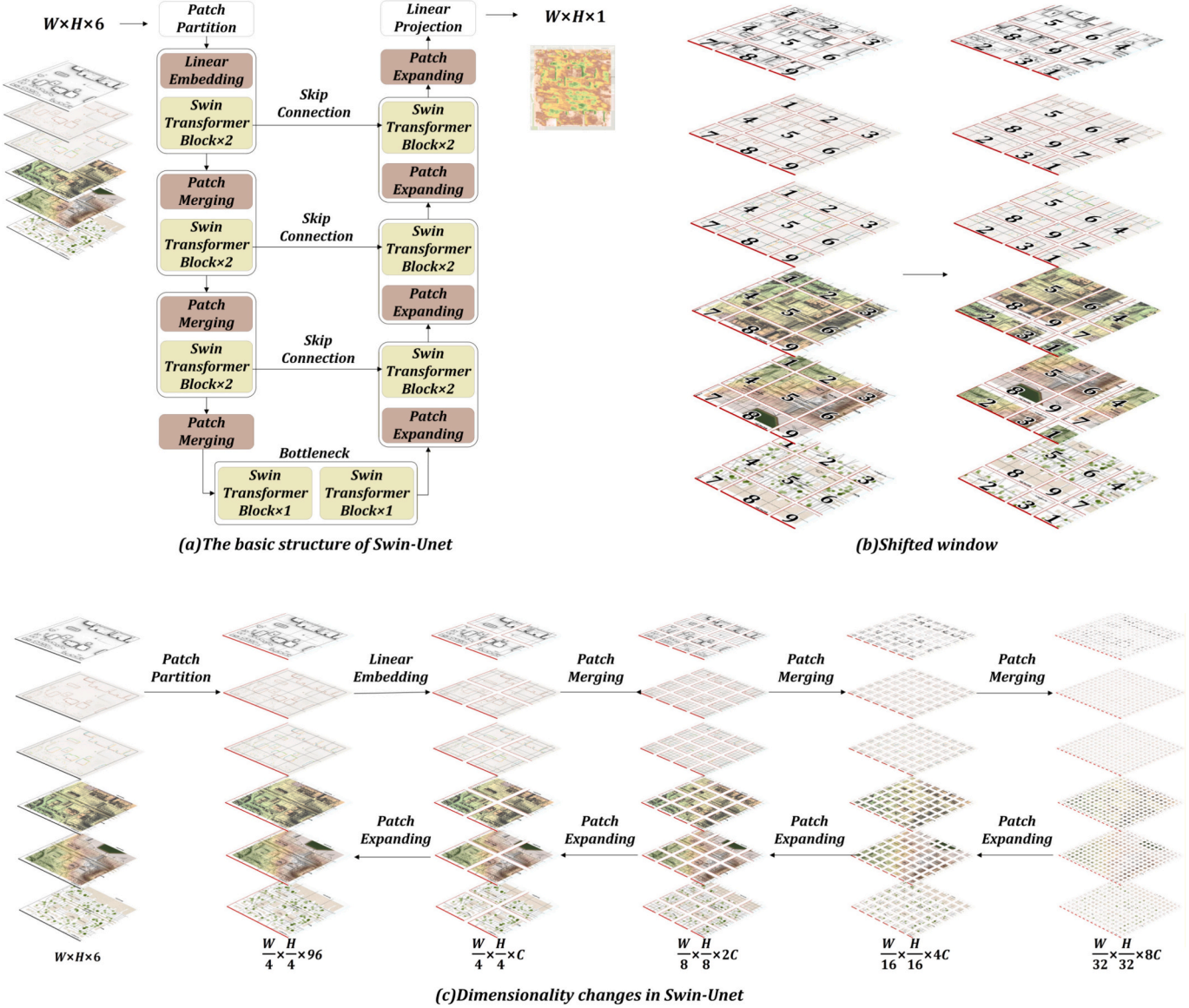

Fig. 5. Swin-Unet architecture.

image segmentation, the model is repurposed here for a regression task by modifying its output layer to generate continuous values. The self-attention mechanism inherent in the Swin Transformer is particularly advantageous, as it directly models the relationships between all input positions. This enables the model to capture the holistic spatial context and cross-regional correlations that are critical for accurately predicting T_{mrt}, which is influenced by interactions across the entire landscape (Cao et al., 2022; Xie et al., 2024).

The Swin-Unet architecture employed in this study is detailed in Fig. 5. The model is configured with six input channels, which contain data on the study area's surface features and tree distribution, and a single output channel that predicts T_{mrt}. It retains the classic U-shaped structure, comprising an encoder path and a decoder path (Fig. 5(a)). However, departing from the standard U-Net, this architecture replaces convolutional blocks with Swin Transformer blocks that utilize a more efficient, window-based self-attention mechanism (Liu et al., 2021). As depicted in Fig. 5(b), this mechanism partitions feature maps into non-overlapping windows and computes self-attention within them, subsequently using a shifted window approach to facilitate information exchange across these partitions. This design enables the model to effectively capture global contextual relationships while maintaining computational tractability.

The flow of data through the network follows a systematic dimensional transformation (Fig. 5(c)). The encoder progressively downsamples the input, reducing spatial resolution while increasing channel depth to extract a hierarchy of abstract, high-level features. Conversely, the decoder path systematically upsamples these features, gradually restoring spatial detail by integrating coarse, deep-level information with fine, shallow-level features from corresponding encoder stages via skip connections. This process ensures that the final prediction is both contextually aware and spatially precise, leveraging the model's ability to synthesize local details and global information (Cao et al., 2022; Falk et al., 2018).

The Swin-Unet model is trained to learn the complex, non-linear relationship between multi-layered input features, including tree distribution and surface characteristics, and the resulting T_{mrt}. As illustrated in Fig. 6, the model processes a six-channel input tensor and generates a single-channel output raster, with both sharing identical spatial dimensions. This architecture effectively frames the simulation as a spatial regression task, where the model predicts a continuous value for each pixel. Accordingly, the model's predictive accuracy, which is also the loss of the Swin-Unet, is quantified using the Mean Squared Error (MSE), a standard metric for regression problems that measures the average squared difference between the predicted and ground-truth values. The MSE is calculated as:

$$MSE = \frac{\left(\|T_{mrt} - \widehat{T_{mrt}}\|_2\right)^2}{N} \tag{4}$$

Among them, $\| \bullet \|_2$ is the L2-norm, T_{mrt} and $\widehat{T_{mrt}}$ are the mean radiant temperature distribution computed using SOLWEIG and the Swin-Unet model trained in this study, respectively. N is the total number of grids in the study area.

Following model training, the performance of models across varying numbers of training epochs is evaluated on both the training and validation sets using the R^2 (coefficient of determination) and MAE (Mean Absolute Error) metrics.

4.2.2. Data preparation

The data preparation workflow creates a large, augmented dataset for Swin-Unet training and validation through a three-stage process (see Fig. 7). First, LiDAR point cloud data for Tucson is processed to create foundational terrain data for 92 sample plots. Next, for each plot, 500

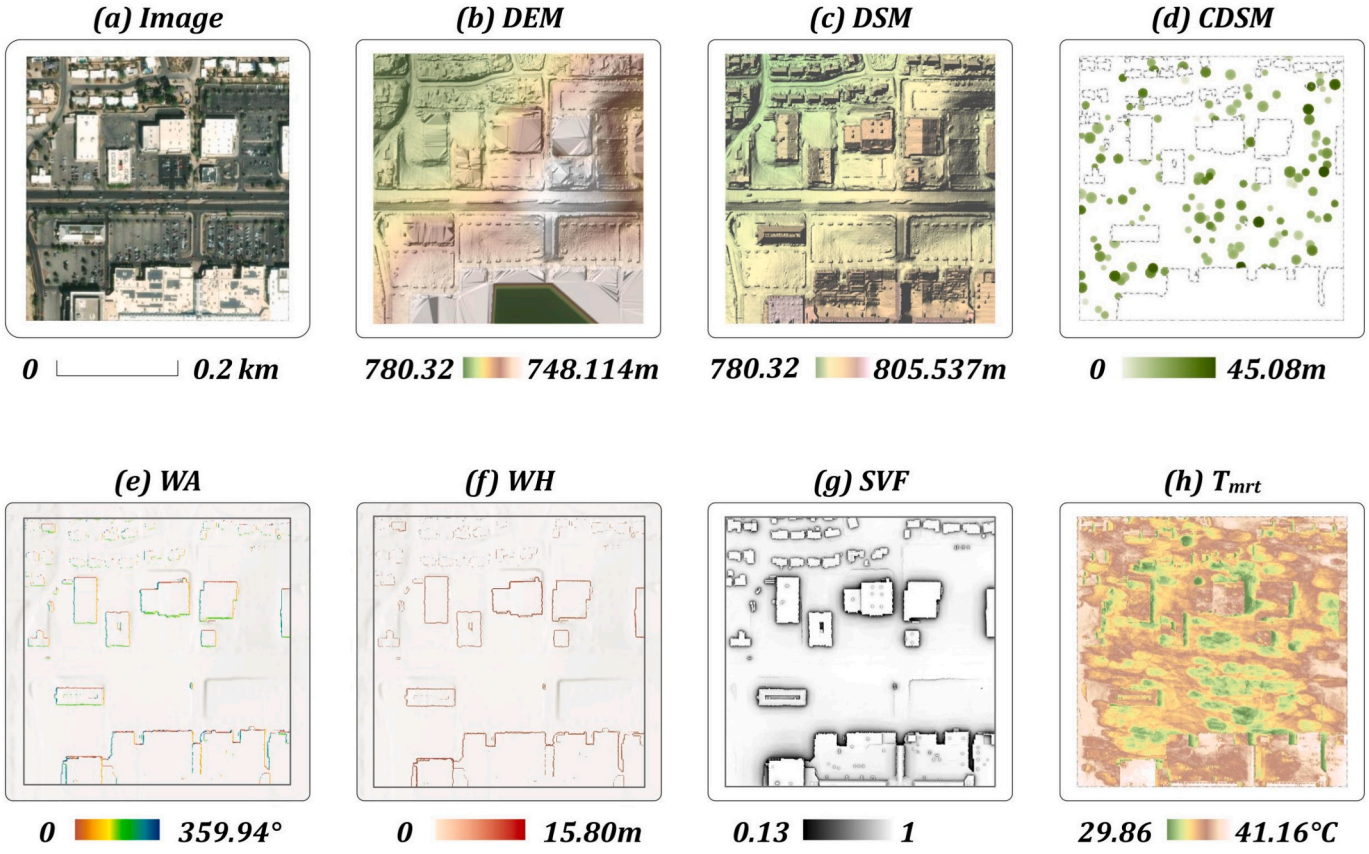

Fig. 6. A sample of the input and output data. Subfigures (a) is the remote sensing image of the sample area, (b)-(g) is the six-channel input data, (h) is the output data.

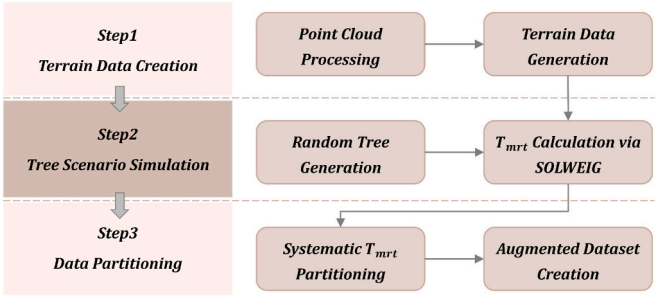

Fig. 7. Data processing workflow.

unique tree distribution are randomly generated and the SOLWEIG model is then used to calculate the mean radiant temperature (T_{mrt}) for every scenario. Finally, a data augmentation strategy is applied where each T_{mrt} output is systematically partitioned into 30 smaller datasets, massively increasing the scale and diversity of the final dataset for model training and validation.

We use LiDAR point cloud data to generate terrain features. The LiDAR data for the study area of Tucson were acquired from the Open Topography platform ((USGS), U. S. G. S, 2023). From this dataset, we established 92 spatially random 500-by-500-m sample plots. Fig. 8(a) illustrates the spatial distribution of the dataset, which was partitioned into training and validation subsets at a 20:3 ratio. The dataset included a variety of land use types, such as residential areas, mixed residential and bare land areas, and mixed residential and commercial areas Fig. 8 (b). This compositional heterogeneity was designed to enhance the robustness of the training process. Each plot was then spatially intersected with the LiDAR data to generate a corresponding point cloud subset for subsequent analysis.

Using ArcGIS Pro, we first classified each point cloud subset into "Building" (e.g., buildings) and "non-Building" classes (Fig. 9(a)). Based on these classifications, we generated a DSM and a DEM for each plot, both at a one-meter spatial resolution. To mitigate edge effects inherent in grid-based analysis, a central 448 × 448-m area was extracted from each 500 × 500-m plot to serve as the effective analysis unit. Finally, these processed data were imported into the Urban Multi-scale Environmental Predictor (UMEP), an add-in in QGIS, to derive key urban morphology parameters, including WH, WA, and SVF.

SVF is a value used to describe the proportion of the sky visible from a point on the ground, ranging between 0 and 1. The calculation process begins with the identification of building areas, specifically by determining regions where the height difference between the DSM and DEM exceeds 2 m. Subsequently, for each grid center, 153 evenly distributed azimuth directions are selected on the horizontal plane to assess sky visibility individually. The algorithm samples outward along each directional ray and determines whether the sky is visible in that direction by comparing the maximum elevation angles of terrain and building obstacles. The results from all directions are then integrated using spherical geometry to obtain the total SVF value for each grid.

The calculation of WH and WA also starts with the extraction of the building mask, which is derived from areas where the height difference between the DSM and DEM exceeds 2 m. WH is calculated by locating the edges of building outlines and taking the difference between the maximum building height inside the outline points and the ground elevation outside. WA is determined by extracting the vector boundaries of building polygons, calculating the outer normal direction of each boundary segment, and converting it into a geographic azimuth angle ranging from 0 to 360 degrees.

To simulate the impact of trees, we designated all non-building areas as feasible for tree planting. Within these zones, we randomly generate 500 unique tree distribution datasets. This number was determined through preliminary experiments, which confirmed that it is sufficient to effectively cover the solution space, ensure stable model convergence, and capture the complex patterns of how variations in trees influence T_{mrt}. In these simulations, individual trees were modeled with a hemispherical morphology, defined by their trunk height and canopy radius, as illustrated in Fig. 9(b). The spatial attributes and morphological parameters for each tree were determined by the following stochastic rules: the number of trees per plot was randomly sampled from a range of 3 to 200; canopy radii were drawn from a uniform distribution between 2 and 10 m; and tree heights were generated from a Gaussian distribution with a mean value set to twice the canopy radius. This parameter configuration is consistent with the specific vegetation morphology determined by the hydrothermal conditions of the study area (Schuch, 2018). It aligns with the structure of the small-sized tree species, such as Arizona cypress (Pourreza et al., 2022) and also conforms to the dimensional characteristics of the medium-to-large-sized tree species, such as ash (Hein & Spiecker, 2008; Meshkova et al., 2024). The resulting raster data for each simulated tree arrangement formed a Canopy Digital Surface Model (CDSM), an example of which is shown in Fig. 9(c). Finally, by integrating the CDSM with the previously generated DEM and DSM, we utilized the SOLWEIG model to calculate the spatial distribution of T_{mrt} across the study areas.

To increase data scale and diversity, this study adopts a multi-stage spatial partitioning strategy on each original 448 × 448-pixel data generated in the previous step. First, orthogonal bipartitioning along both axes divides the image into four non-overlapping 224 × 224 subunits (denoted as $Q_1 - Q_4$ in Fig. 10(a)). Then, a fifth subunit (C in Fig. 10(b)) is cropped from the center. Additionally, a sliding window of size 224 × 224 is applied, randomly generate 25 distinct cropping

Fig. 8. Dataset for training the Swin-Unet model.

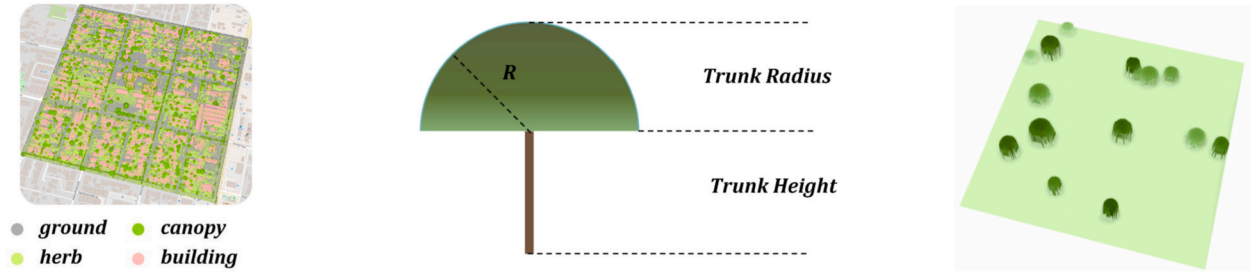

(a) Point cloud classification results (b) Parameter settings during the tree generation process (c) CDSM data diagram

Fig. 9. Terrain and tree simulation data generation.

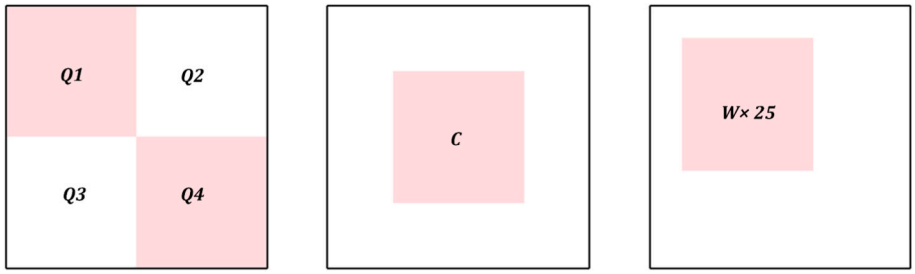

(a) Orthogonal bipartitioning (b) Center cropping (c) Sliding window cropping

Fig. 10. Data partitioning methods.

regions (W in Fig. 10(c)). This process will generate 30 subunits per original dataset.

Ultimately, the training dataset contains 1,200,000 samples. The validating dataset contains 180,000 samples. Additionally, we prepared a separate test dataset that contains 30 plots with the same method. The test dataset does not spatially overlap with the training and validation dataset.

4.2.3. Model training

Given the significant convergence challenges associated with training Swin-Unet's Swin Transformer blocks from scratch, this study initialized each block with weights from a pre-trained model. Specifically, we adopted the "swin_tiny_patch4_window7_224.pth" model provided by Microsoft for this purpose (Liu et al., 2021; Microsoft, 2021). The corresponding hyperparameters and training environment are specified in Table 1.

4.3. Tree location optimization

To optimize tree locations while mitigating the computational demands of high-resolution grid data, this study implements a hierarchical, two-stage framework. We first established a macro-scale for analysis by downscaling the original 224 × 224 grid using a block aggregation strategy. In this strategy, each 4 × 4 block of grid cells (16 cells) is consolidated into a single spatial unit, with the central cell designated as its representative location. This procedure compresses the grid to 56 × 56 spatial units—a fourfold reduction in resolution—which serves as the basis for the macro-unit optimization phase (Fig. 11). During this phase, a genetic algorithm identifies optimal planting locations at the macro-unit level, assuming the trees are planting at the representative location of the corresponding macro-unit. Subsequently, the micro-scale stage refines these placements through fine-grained, grid-level positional adjustments within the selected units, thereby achieving a robust multi-scale collaborative optimization.

In the macro-unit optimization phase, a solution s' is still a set of k locations $p^{(1)}, p^{(2)}, \ldots, p^{(k)}$. For each $p^{(i)} = (r_i, c_i)$, the coordinate must be within the within the 224 × 224 spatial range and satisfies:

$$(r_i + 1) \equiv 0 \ (mod\ 4) \& (c_i + 1) \equiv 0 \ (mod\ 4) \tag{5}$$

Subsequently, a genetic algorithm is employed for a global search, where each s' serves as an individual in the genetic algorithm. Since we are trying to maximize T_{mrt} reduction, or in another word minimize T_{mrt}, the fitness function of genetic algorithm can be defined as the opposite number of the mean T_{mrt}, which is obtained through the trained Swin-Unet model (Fig. 12(a)):

$$f(s') = -\overline{T_{mrt}}(s') \tag{6}$$

We implemented a genetic algorithm driven by crossover, mutation, and selection operators (Fig. 12(b)). To foster population diversity, we employed a two-point crossover strategy, which exchanges chromosome segments between two randomly chosen cut points in parent solutions. Our hybrid mutation operator balances exploration and exploitation: a global mutation (70% probability) relocates a tree to an unoccupied position, while a local perturbation (30% probability) applies a random integer offset within [−5, 5] to a tree's coordinates. Finally, the selection process combines tournament selection with an elitist strategy to

Table 1
Training environment and hyperparameters.

Category	Parameter Name	Value / Setting
Environment	GPU Version	2 × NVIDIA GeForce RTX 4090
	RAM	256G
	CPU Version	40-core vCPU @ 3.00GHz
	CUDA Version	12.1
	VRAM (Total)	48 GB
	Python Version	3.11.10
Batch	Batch Size	64
Optimizer	Type	Adam
	Initial Learning Rate	0.001
Learning Rate Schedule	Adjustment Mechanism	Dynamic Decay
	Decay Factor	0.1
	Decay Schedule	Not Specified
Reproducibility	Random Seed	1234

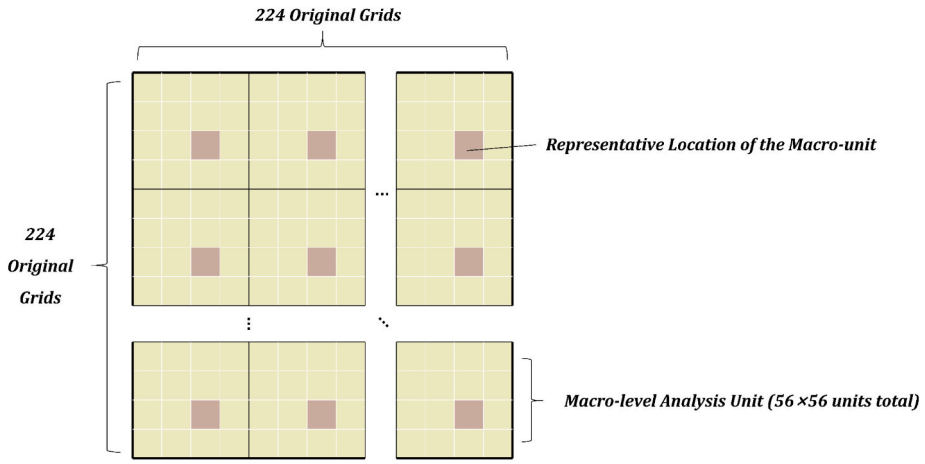

Fig. 11. Hierarchical grid downscaling for tree optimization.

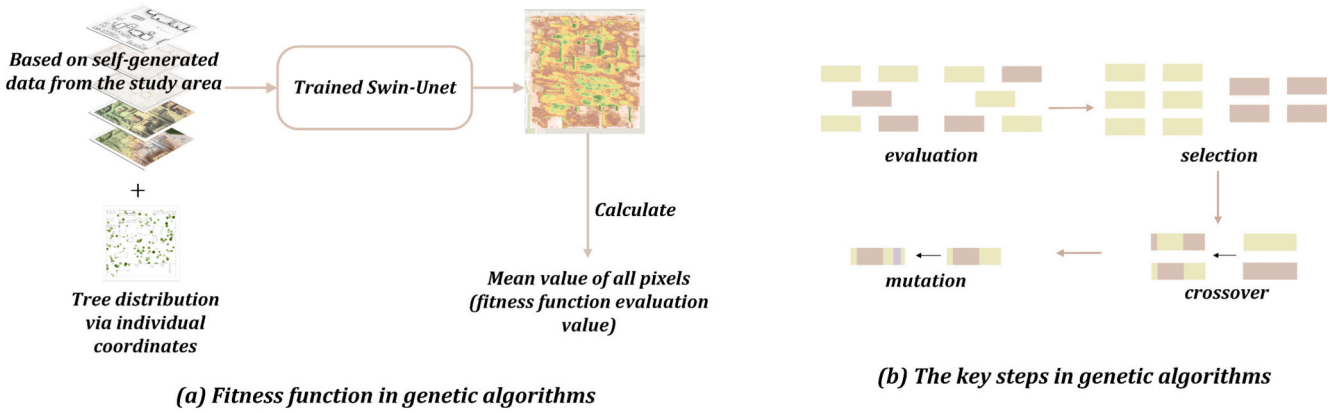

Fig. 12. Genetic algorithm for tree location optimization

guarantee that the best-performing solutions advance to the next generation.

Following the genetic algorithm's global search, a local refinement stage fine-tunes individual tree placements. For each tree in the optimized configuration, the algorithm exhaustively evaluates all 16 grid cells within its 4 × 4 macro-unit as potential new locations. While holding all other tree positions constant, it repositions the target tree to each candidate cell and selects the location that yields the lowest $\overline{T_{mrt}}$. This iterative process cycles through every tree in the solution until a dual-threshold termination condition is met: the algorithm halts if the improvement in the objective function between consecutive cycles is less than 0.0001 or after completing 10 full cycles. The resulting configuration represents the final optimized solution.

5. Test results

This study applies the proposed optimization method to a case study in Tucson, Arizona, USA. The primary objective is to minimize T_{mrt} during the city's hottest day in 2023, thereby testing the model's effectiveness at mitigating extreme heat conditions.

5.1. Accuracy evaluation of Swin-Unet

Fig. 13 illustrates the MSE loss curves for the training and validation sets. The model demonstrated effective convergence by approximately epoch 30, with the training MSE stabilizing at 0.96 and the validation MSE at 1.06. We concluded the training process at epoch 55, selecting the final model state from this epoch for all subsequent analyses.

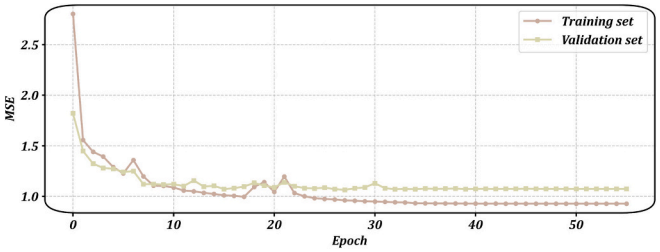

Fig. 13. Training and validation loss.

Furthermore, we conducted a comprehensive evaluation of the training, validation, and test datasets utilizing the definitive 55-round model employed in this study. The corresponding performance metrics are summarized in the Table 2 below.

To evaluate computational performance, we benchmarked the single-inference time of our trained Swin-Unet model against the established SOLWEIG model. Averaged over 100 randomized runs, the Swin-Unet model required only 1.9 s per inference, compared to 32 s for SOLWEIG (Fig. 14). This result represents a 17-fold acceleration in

Table 2
Model performance across datasets.

	Training set	Validation set	Testing set
R^2	0.8287	0.8029	0.7688
MAE	0.7475	0.8000	0.8155

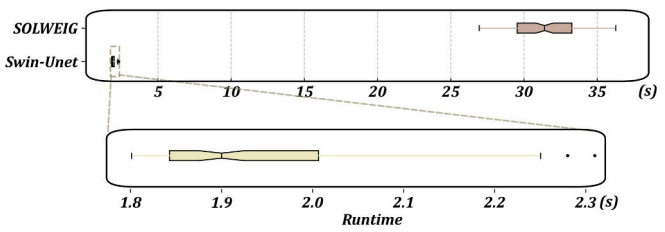

Fig. 14. Computational time comparison: Swin-Unet vs SOLWEIG.

inference speed, highlighting the deep learning model's significant efficiency advantage.

To validate the predictive accuracy of the Swin-Unet model, a test was conducted in a representative residential neighborhood bounded by E. North Street and N. Walnut Avenue (Fig. 15(a)). For this area, a validation dataset was generated comprising 1000 random tree layouts, each containing between 5 and 30 trees with a canopy radius and trunk height of 5 m. The SOLWEIG model was employed to calculate the ground-truth T_{mrt} for each configuration, providing a benchmark against which the Swin-Unet predictions were evaluated. The comparison revealed strong model performance: For 90% of the test cases, the mean relative spatial error in T_{mrt} was confined to a narrow range of −3.60% to 3.07%, with an average MSE of 1.039 (Fig. 15(c)). The accumulated spatial errors distribution indicated that larger discrepancies were primarily concentrated in close proximity to building facades (Fig. 15(b)). Although this suggests an area for future model refinement, subsequent experiments confirmed that these localized inaccuracies had a negligible impact on the overall efficacy of the spatial optimization algorithm.

To assess the model's robustness and stability across different tree size, its predictive performance was further evaluated under three distinct scenarios: tall trees (5 m canopy radius, 8 m trunk height), short trees (5 m canopy radius, 3 m trunk height), and large trees (8 m canopy radius, 8 m trunk height). Following the same validation methodology, we quantified the MSE for each scenario to determine how tree size and form influence prediction accuracy. The MSEs for tall trees, short trees and large trees are 1.055, 1.026, 1.085, indicating consistent performance over different tree sizes. Specifically, the optimization time of SU-MHGA remained stable within the range of 865 to 885 s across different tree sizes, whereas the computational cost of TreePlanter increased sharply with tree size, exceeding 30,000 s for large trees. Meanwhile, the layout generated by SU-MHGA achieved lower mean radiant temperature across all sizes, with a spatial pattern that tends to enhance shading effects through dispersed planting and proximal arrangement near buildings, demonstrating superior robustness and adaptability (see Appendix B for detailed results).

5.2. Tree location optimization

5.2.1. Cooling effect comparison

Upon successful training, the Swin-Unet model was deployed to optimize tree layouts within standardized 224 m × 224 m plot containing target community. The optimization was executed using the previously described genetic algorithm, configured with a population size of 2048 and run for 300 generations. To benchmark the SU-MHGA, we performed a comparative analysis against TreePlanter, a state-of-the-art tool that employs a hill-climbing algorithm for tree placement optimization.

To demonstrate the practical application and comparative performance of SU-MHGA, the calculation continues using the same position as in Fig. 15 (denote as Area A, Fig. 16(a)). The experiment systematically evaluated optimal tree layouts for scenarios where the total number of trees (k) ranged incrementally from 5 to 15. The final configurations produced by both the proposed genetic algorithm and the baseline TreePlanter were then assessed using the SOLWEIG model to calculate the $\overline{T_{mrt}}$ for each outcome. A comparison of the cooling effectiveness of the two methods across different numbers of trees, measured using the $\overline{T_{mrt}}$ value, is shown in Fig. 16(b). Specifically, SU-MHGA consistently outperforms the TreePlanter in all test cases, achieving an additional temperature reduction of 0.0831 °C at most and 0.0286 °C at least.

A comparative analysis of the resulting layouts reveals fundamental divergences between the two approaches (Fig. 17). The TreePlanter consistently produces schemes characterized by a high degree of spatial clustering, where trees are densely concentrated within specific, often open, areas. In contrast, the method proposed herein generates a markedly more dispersed spatial pattern, in which trees are distributed with greater uniformity throughout the study area and are sometimes preferentially sited in proximity to buildings.

This fundamental difference in spatial distribution is the primary determinant of the divergent cooling performance observed between the two methods. Tree configurations concentrated in open areas, as produced by the TreePlanter, yield highly localized shade canopies that provide limited direct solar protection for surrounding building facades. Conversely, the dispersed layouts generated by SU-MHGA, particularly with trees sited near buildings, offer more extensive and strategically positioned shading. This placement more effectively mitigates solar heat gain on building surfaces and within adjacent spaces, thereby improving localized thermal comfort. Consequently, the strategic principles guiding our optimization—dispersion and building proximity—are

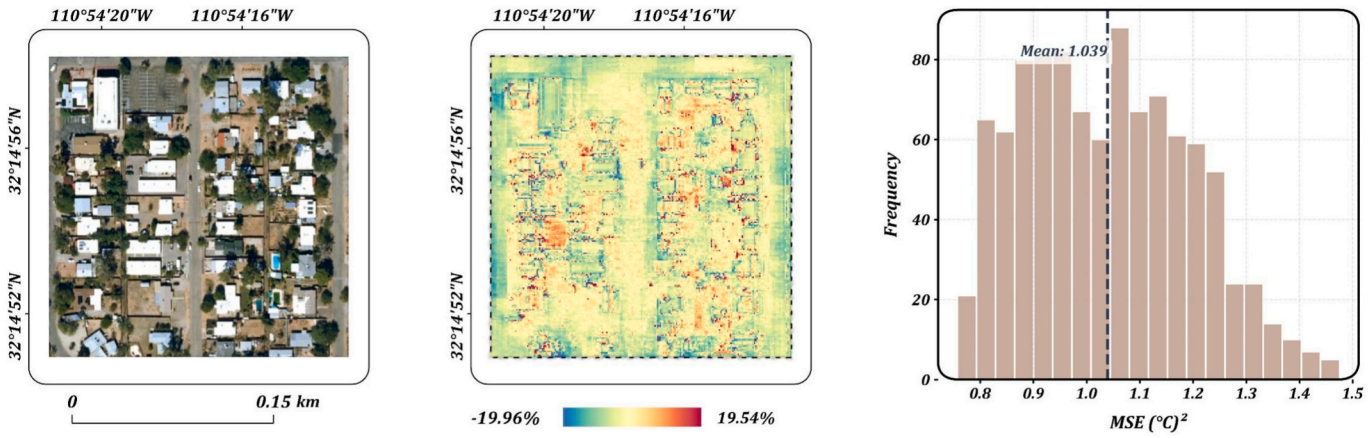

Fig. 15. Spatial relative error distribution of a sample area.

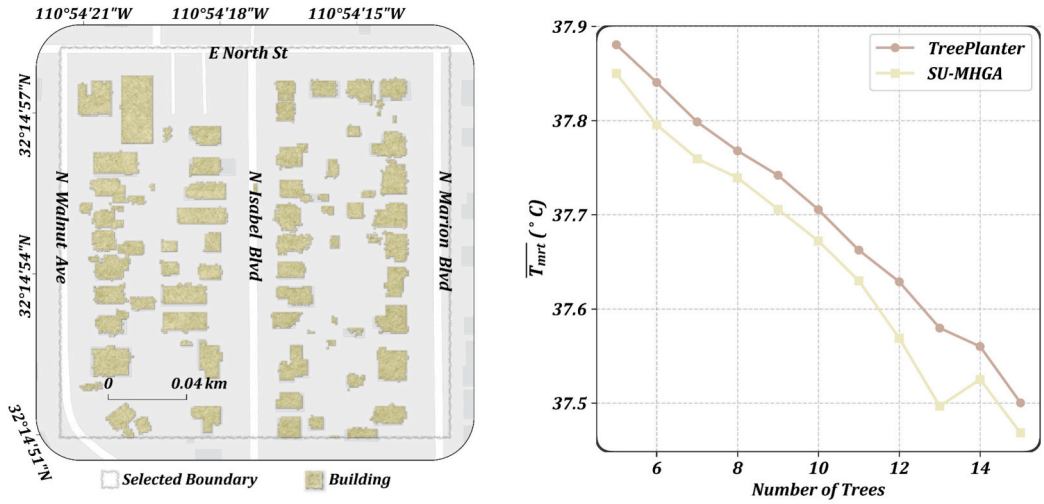

Fig. 16. Cooling effect comparison between SU-MHGA and TreePlanter.

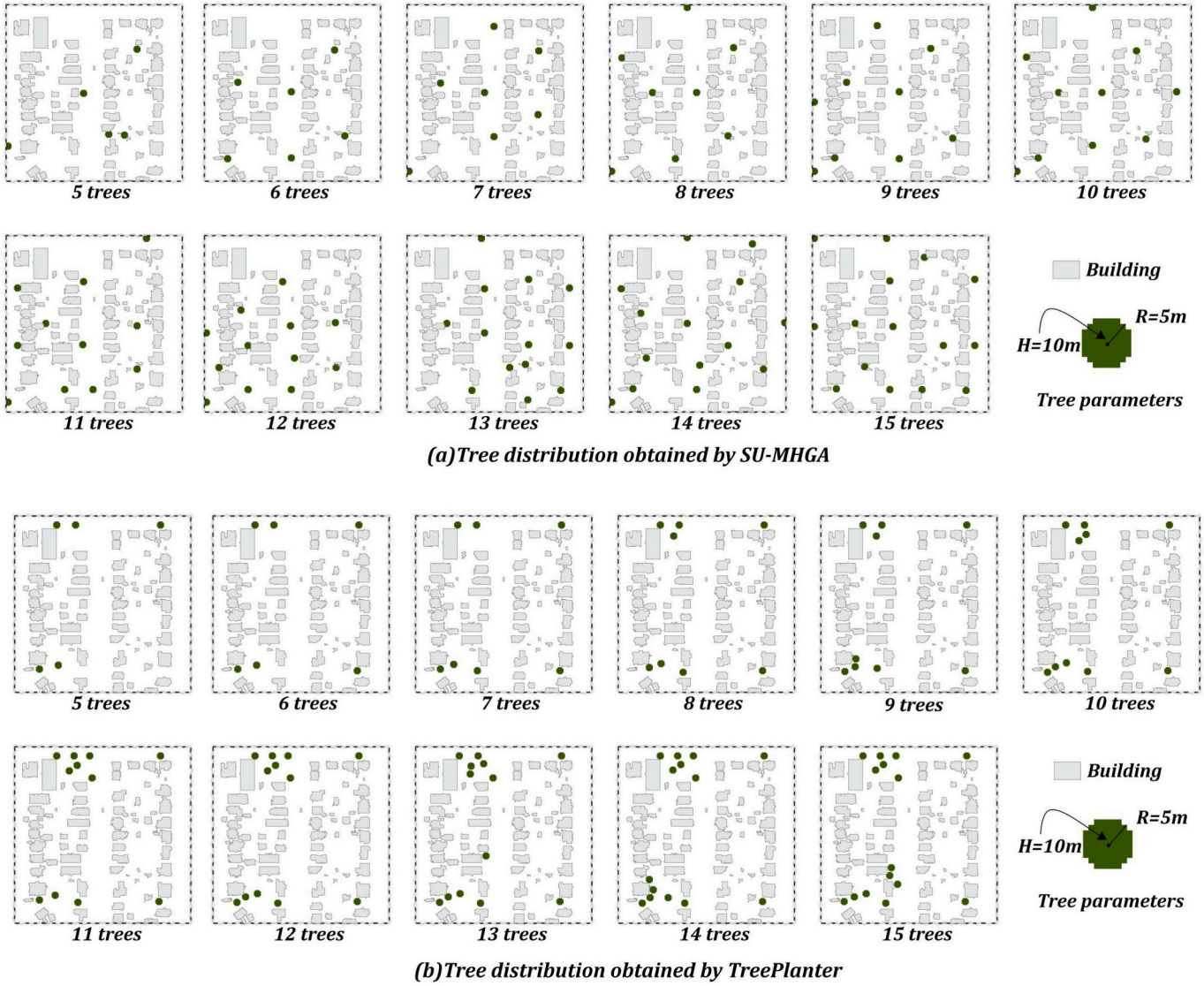

Fig. 17. Optimal tree distribution generated by SU-MHGA and TreePlanter in Area A.

demonstrably more effective for achieving comprehensive and balanced microclimate regulation.

In accordance with the No Free Lunch Theorem, which posits that the efficacy of any heuristic optimization algorithm is inherently context-dependent, which means no single heuristic optimization algorithm can universally outperform all others across every problem domain (Wolpert & Macready, 1997), a comprehensive validation was conducted to assess the stability of performance of SU-MHGA. This analysis involved a comparative study across 30 diverse urban communities, including residential areas, commercial centers, and school campuses. Within each area, the difference in $\overline{T_{mrt}}$ was calculated for 5-tree layouts generated by both SU-MHGA and the TreePlanter. The findings, detailed in Fig. 18, reveal a decisive advantage for the proposed method, which yielded superior cooling performance in 28 of the 30 tested locations.

5.2.2. Cross-year transferability validation

To validate the temporal transferability of the SU-MHGA method, this study further examined the model's performance under extreme heat events in different years. From a temporal perspective, the core objective of this study is to optimize urban tree layouts for extreme heat scenarios. Therefore, the hottest day of 2023 was selected as the representative extreme scenario for training the model. Research has demonstrated that despite inter-annual variability in specific meteorological values, the relative stability of spatial determinants governing surface energy balance results in reproducible spatial patterns of T_{mrt} at local microclimate scales (Yun et al., 2023). This implies that although the absolute values of meteorological data may fluctuate between years, the spatial distribution patterns of T_{mrt} and the cooling effects of trees remain relatively consistent.

Furthermore, considering the practical challenges in model construction, prior studies have pointed out that directly incorporating dynamic meteorological inputs often introduces significant uncertainty, which can severely compromise model accuracy and predictive reliability (Briegel et al., 2023). Therefore, after weighing these factors, this study established the following design rationale: under the premise of keeping computational complexity manageable, priority is given to ensuring robust optimization performance under the targeted extreme scenario.

To verify the above assumption, we compared the spatial distribution of T_{mrt} under treeless conditions on the hottest days of 2023 and 2024. As shown in Fig. 19 (daily average results), the relative spatial patterns of T_{mrt} were highly consistent between the two years, supporting the rationality of the scenario selection in this study.

On this basis, we further used the 2024 climate data to generate corresponding tree layout optimization plans using TreePlanter. Comparing the original plan of this study with the new TreePlanter plan based on the 2024 climate background (Fig. 20), it was found that even under the 2024 climatic conditions, the SU-MHGA plan proposed in this study still outperformed the TreePlanter plan in reducing $\overline{T_{mrt}}$, indicating that the proposed method possesses a valid cross-year extrapolation capability. (See Fig. 21.)

5.2.3. Computational time

To evaluate computational performance, the proposed method was benchmarked against the TreePlanter algorithm across three distinct neighborhood, Area A as mentioned before, and two other community Area B and C. The computational time required to site between 5 and 15 trees was recorded for both approaches (Fig. 22). The analysis revealed that SU-MHGA exhibits superior computational efficiency and stability, with runtimes consistently falling within a narrow range of 865 to 890 s. In stark contrast, the performance of TreePlanter degraded significantly as the problem scale increased, demonstrating high volatility and unpredictable processing durations. This instability culminated in an extreme case where the time required to place 15 trees exceeded 120,000 s (approximately 33.3 h). These findings underscore that SU-MHGA offers a computationally robust and scalable solution, whereas TreePlanter is highly sensitive to problem complexity and regional characteristics, rendering it impractical for larger or more intricate optimization tasks. We provide the detailed optimization results for Area B and C in the Appendix.

Furthermore, a direct comparison of computational efficiency for the 5-tree planting scenario across the 30 previously examined regions reinforces this conclusion (Fig. 23). SU-MHGA consistently demonstrated rapid performance, with runtimes clustering around 869 s, with a MSE 6.13. In contrast, the TreePlanter algorithm required substantially more time, averaging approximately 17,000 s, with a MSE 2.39×10^7 for the same task, which further substantiates the computational stability and efficiency of SU-MHGA.

6. Discussion

This study successfully demonstrates a novel and highly efficient framework, SU-MHGA, for optimizing urban tree placement to mitigate extreme heat, addressing critical limitations of existing methods. The integration of a Swin-Unet metamodel with a multiscale hybrid genetic algorithm proves to be a powerful combination, delivering superior

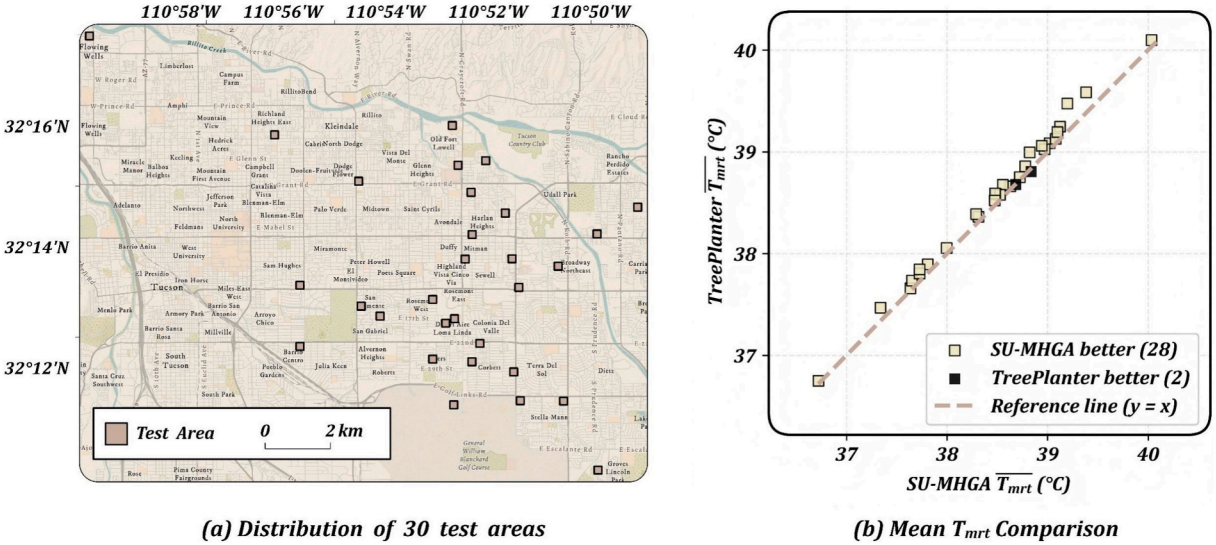

(a) Distribution of 30 test areas *(b) Mean T_{mrt} Comparison*

Fig. 18. Comparison of $\overline{T_{mrt}}$ at 30 randomly selected area between SU-MHGA and TreePlanter.

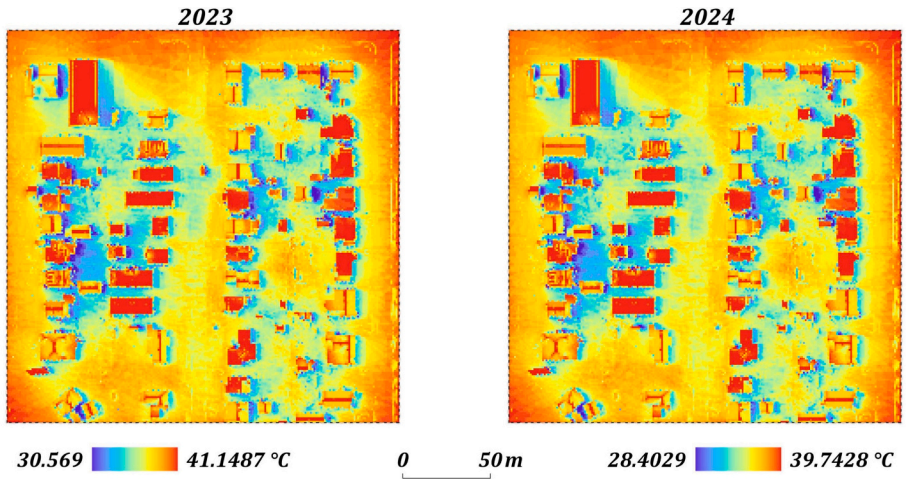

Fig. 19. Comparison of the daily average T_{mrt} between the hottest day in 2023 and the hottest day in 2024.

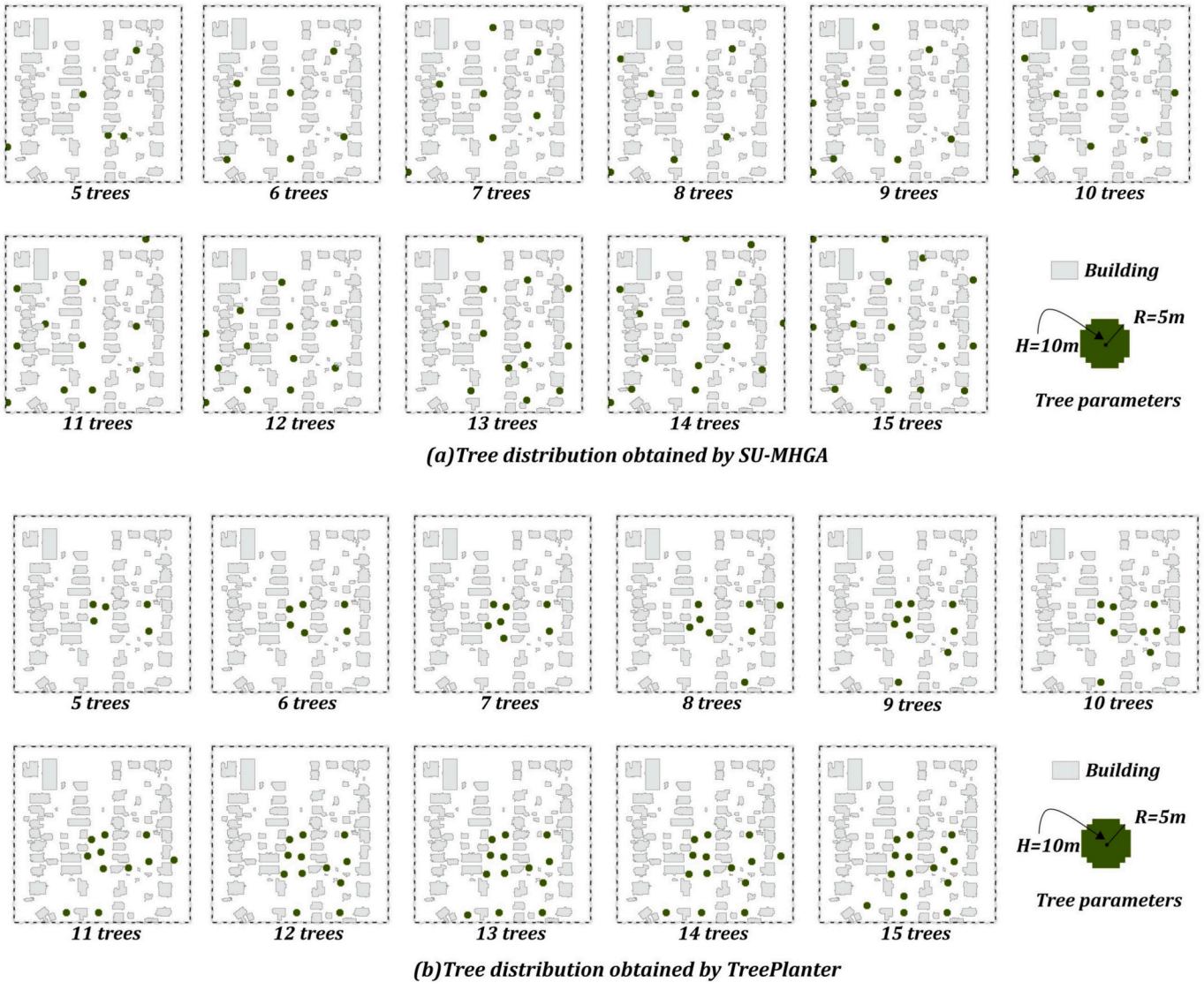

Fig. 20. Spatial optimization scheme for TreePlanter based on climate factors from the hottest day of 2024, and its differences from the SU-MHGA scheme.

cooling outcomes with a fraction of the computational time of conventional tools.

A key finding of this research is that the Swin-Unet model can serve as an exceptionally fast and accurate surrogate for the physically-based

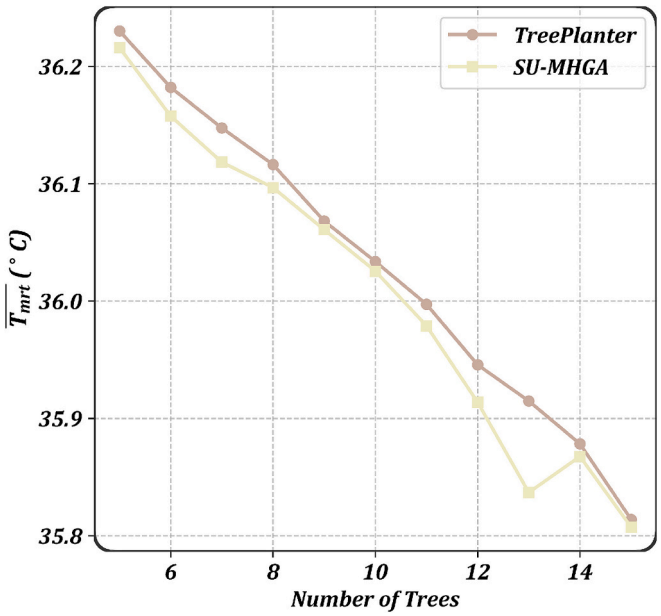

Fig. 21. Comparison of $\overline{T_{mrt}}$ between two optimization algorithms based on calculations for the hottest day of 2024.

SOLWEIG model. Its high predictive accuracy, coupled with a 17-fold acceleration in inference speed, is not merely an incremental improvement; it is what makes the use of a sophisticated genetic algorithm computationally feasible for a complex spatial problem. This efficiency unlocks the ability to evaluate thousands of candidate tree layouts, a task that would be intractable using the SOLWEIG model directly. The strategic advantage of SU-MHGA—achieving demonstrably better cooling results than the TreePlanter benchmark—is fundamentally enabled by this high-speed, high-fidelity metamodel.

This study corroborates the findings of Manickathan et al. (2018) who observed that the marginal cooling efficiency of vegetation diminishes as tree density increases excessively. This saturation effect underscores the critical necessity of optimizing spatial arrangement rather than merely increasing biomass. Regarding model architecture, the Swin-Unet employed here achieved a MAE of approximately 0.8 K on both validation and test sets. This represents a significant improvement over previous U-Net benchmarks, which reported deviations around 2.4 K (Briegel et al., 2023), thereby demonstrating our model's superior generalization capability in extrapolation tasks. In terms of feature selection, we drew upon established correlations between solar radiation and microclimatic variance (Hamed et al., 2023), as well as the governing influence of wind speed on relative humidity (Al-Ramadan et al., 2024). Consequently, we utilized fixed, extreme high-temperature meteorological data for training to stress-test the optimization under critical heat stress conditions. By expanding the search space, our framework achieves cooling outcomes superior to baseline methods like TreePlanter, which often plant trees in already-shaded zones (Wallenberg et al., 2022). However, as Kim et al. (2024) indicate, strategic planting within a certain range of shaded building facades can enhance local cooling effects, and this nuanced variation in specific locations is effectively captured by our global optimization strategy.

Comparative analysis reveals a critical insight into urban cooling strategies. The TreePlanter algorithm consistently produced spatially clustered layouts, which concentrate shade in open areas but provide limited thermal benefit to the surrounding built environment. In contrast, SU-MHGA generated more dispersed patterns that strategically positioned trees near buildings. This approach yields superior cooling by more effectively shading building facades and hardscapes, which are primary sources of absorbed and re-radiated heat. This result empirically validates the principle that for maximizing microclimate regulation in dense urban settings, widespread and strategically placed shading is more effective than concentrated canopy cover.

The optimization framework is characterized by its significant versatility. While the current implementation targets the minimization of mean T_{mrt}, the underlying structure can be readily adapted to optimize for other critical thermal indicators, such as Physiological Equiv-

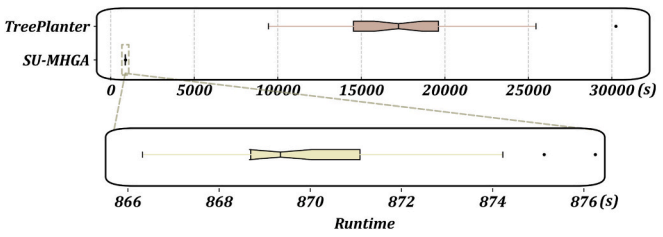

Fig. 23. Computational time of the SU-MHGA and TreePlanter in 30 regions.

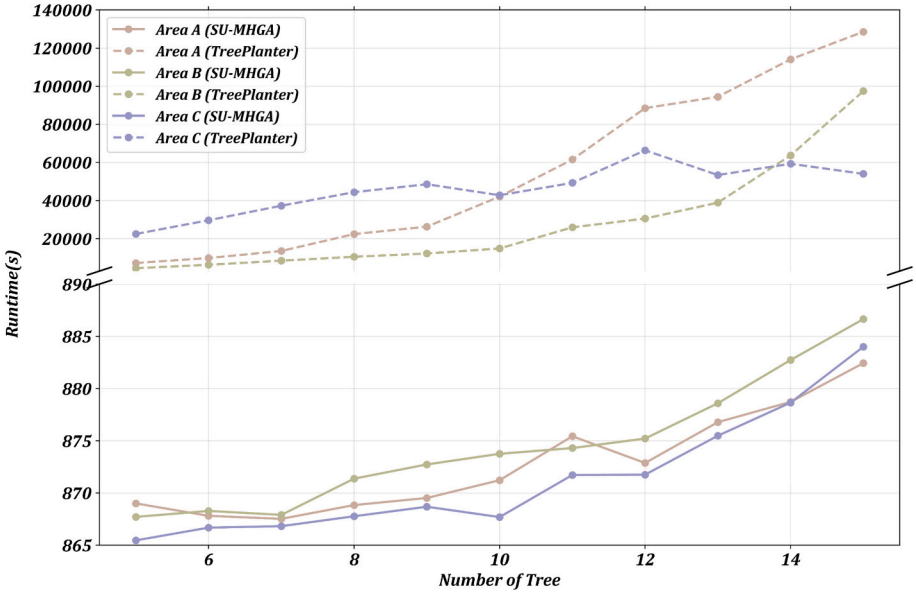

Fig. 22. Computational time of the SU-MHGA and TreePlanter with 5 to 15 trees.

alent Temperature (PET) or Universal Thermal Climate Index (UTCI), or to pursue different statistical goals like minimizing the maximum T_{mrt} in vulnerable areas. The model inherently supports complex scenarios, allowing for the variable definition of tree attributes (e.g., canopy radius, trunk height) and the mixed placement of different tree species. For larger domains, a tiling methodology can be employed to integrate optimized layouts from contiguous sub-regions. This adaptability ensures the framework can be tailored to diverse planning contexts, from residential communities to linear landscapes like street canyons and transportation corridors.

To ensure a focused analysis, several assumptions were made. Climatic factors and ground cover were treated as uniform, and planting was permitted in all non-building areas. This was primarily due to the unavailability of land use datasets with a spatial resolution matching that of this study for the region. Using coarser-resolution data to mask out unsuitable planting areas would introduce spatial errors and compromise the effectiveness of spatial optimization. Furthermore, by adopting the foundational SOLWEIG model, this study inherits its key simplifications, neglecting dynamic factors such as thermal inertia, heat storage in materials, and the evapotranspiration effects of trees on ambient air temperature and humidity (Lindberg et al., 2008). While these assumptions do not detract from the demonstrated superiority of the optimization method itself, integrating these more complex physical processes represents a significant and exciting avenue for future research. Such advancements would further enhance the model's realism and expand its applicability for designing climate-resilient cities.

7. Conclusion

This study addressed the critical challenge of optimizing urban tree placement for thermal comfort, a task often hindered by the prohibitive computational cost of traditional microclimate models. We introduced and validated an innovative framework that integrates a deep learning-based metamodel (Swin-Unet) with a genetic algorithm to efficiently identify optimal tree layouts for mitigating extreme heat.

The primary contribution of this research is the development of a practical, scalable, and data-driven framework that bridges the gap between high-fidelity environmental simulation and real-world urban planning. By drastically reducing computational barriers, this framework empowers urban planners, landscape architects, and policymakers to move beyond intuitive design principles and systematically optimize green infrastructure for maximum climate resilience. As cities worldwide confront the escalating threat of extreme heat, the ability to rapidly design, test, and implement effective cooling strategies is paramount. This work provides a powerful new tool to aid in the creation of more sustainable, equitable, and thermally comfortable urban environments.

Despite these advantages, the model's generalizability and regional adaptability present opportunities for further development. The current framework was trained and validated exclusively on a dataset from a single metropolitan area (Tucson, Arizona), and its performance across diverse geographical and climatic contexts has not yet been verified. Future research should therefore prioritize expanding the geographic scope of the training data. Such an effort is essential for developing robust and widely applicable urban landscape planning tools capable of addressing varied environmental conditions.

CRediT authorship contribution statement

Yuhong Bai: Writing – original draft, Visualization, Methodology, Investigation, Formal analysis, Data curation. **Wangshu Mu:** Writing – review & editing, Writing – original draft, Methodology, Investigation, Funding acquisition, Formal analysis, Conceptualization. **Changqing Song:** Writing – review & editing, Writing – original draft, Investigation, Funding acquisition, Conceptualization.

Author statement

We the undersigned declare that this manuscript is original, has not been published before and is not currently being considered for publication elsewhere. We confirm that the manuscript has been read and approved by all named authors and that there are no other persons who satisfied the criteria for authorship but are not listed. We further confirm that the order of authors listed in the manuscript has been approved by all of us. We understand that the Corresponding Author is the sole contact for the Editorial process. He/she is responsible for communicating with the other authors about progress, submissions of revisions and final approval of proofs.

Acknowledgments

This research was funded by the National Key R&D Program of China (Grant No. 2022YFC3800105), and the National Natural Science Foundation of China (Grant No. 42301476). We would also like to thank the Center for Geodata and Analysis, Faculty of Geographical Science, Beijing Normal University, for their high-performance computing support. Any opinions, findings, and conclusions or recommendations expressed in this material are those of the authors and do not necessarily reflect the views of the funding agencies.

Appendix A. Optimization plan and effect for the other two areas

Mean radiant temperature performance in the other two regions mentioned in the time section and tree planting plans.

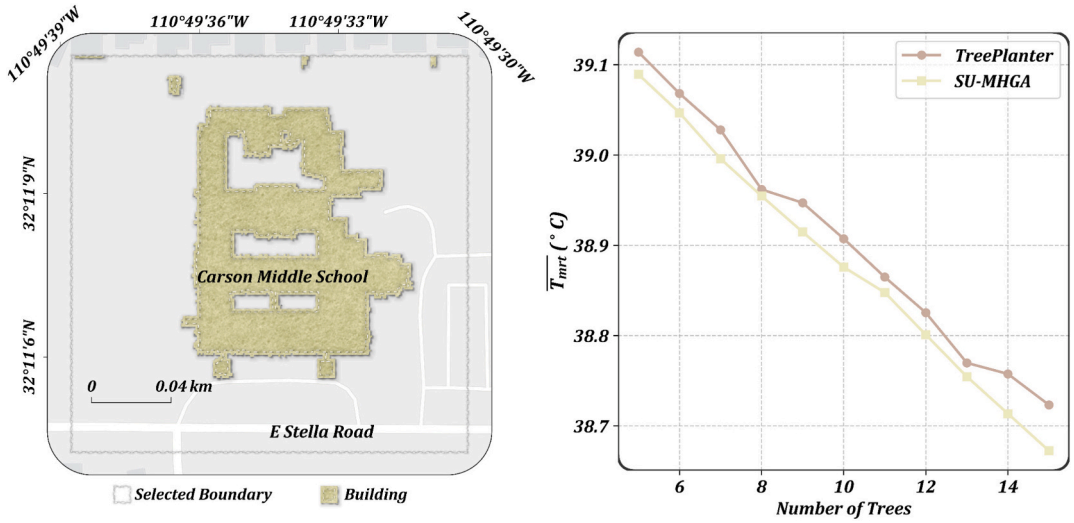

(a) Selected sample area *(b) $\overline{T_{mrt}}$ of the SU-MHGA and TreePlanter*

Fig. 24. Area B: Basic situation of the area and the difference in $\overline{T_{mrt}}$ among different tree numbers.

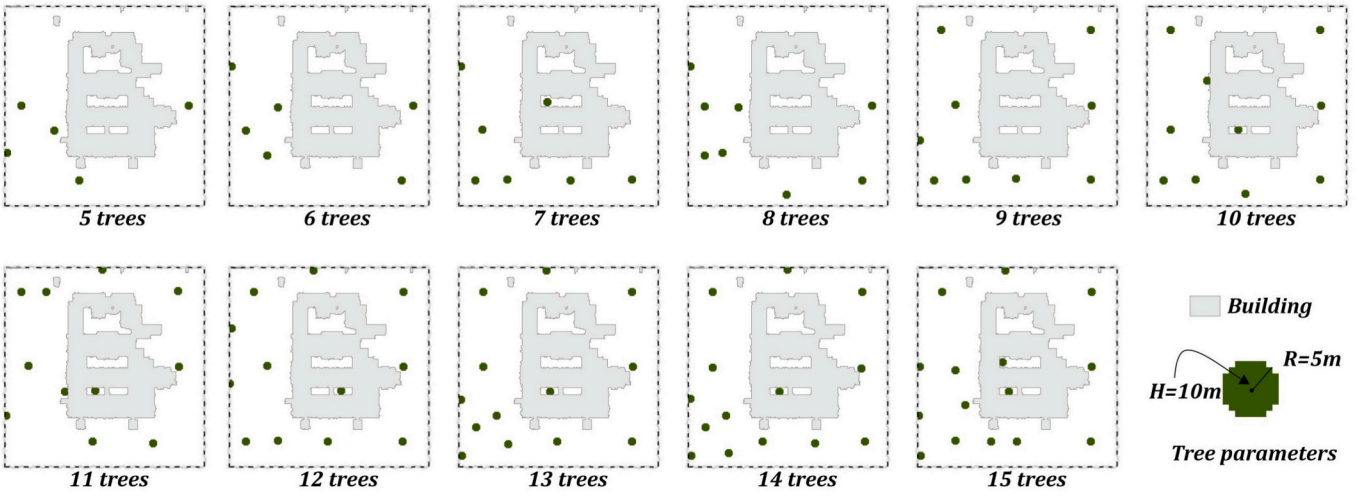

(a)Tree distribution obtained by SU-MHGA

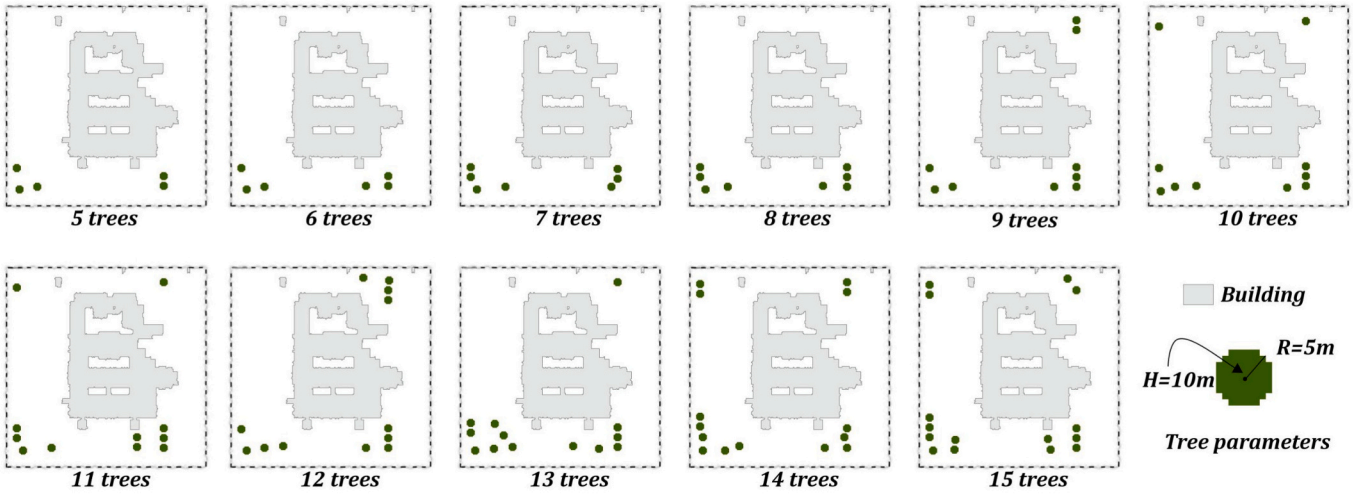

(b)Tree distribution obtained by TreePlanter

Fig. 25. Optimal tree locations by SU-MHGA and TreePlanter in Area B.

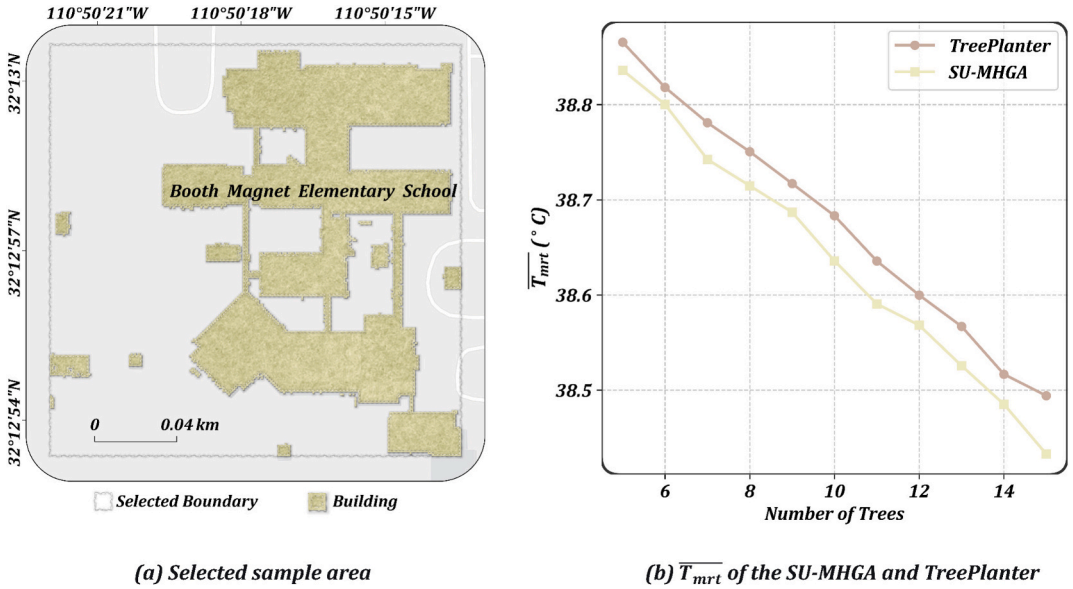

(a) Selected sample area *(b) $\overline{T_{mrt}}$ of the SU-MHGA and TreePlanter*

Fig. 26. Area C:Basic situation of the area and the difference in $\overline{T_{mrt}}$ among different tree numbers.

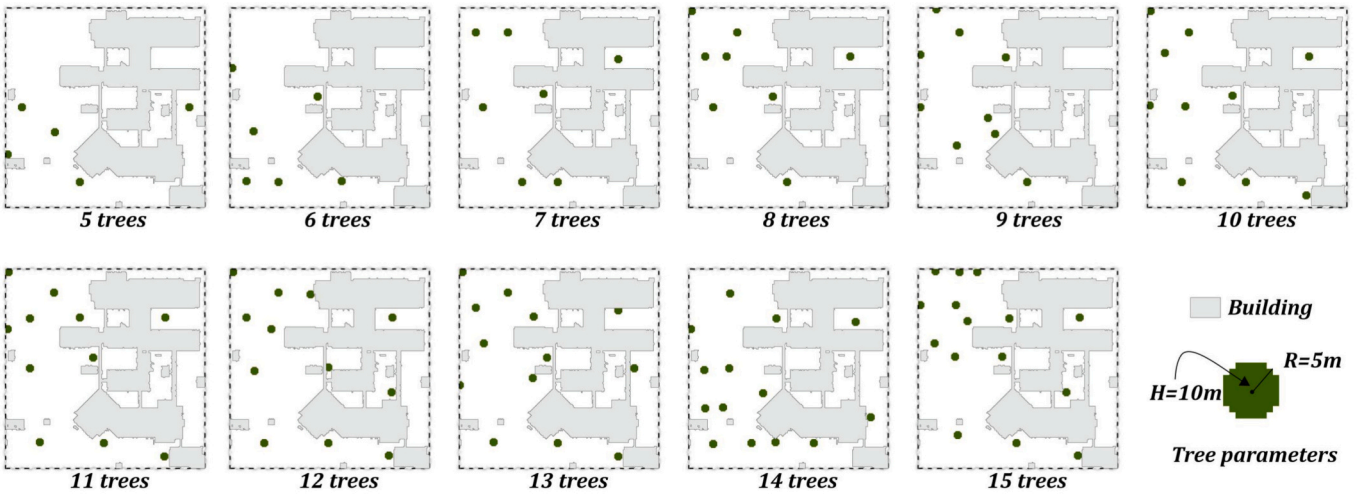

(a)Tree distribution obtained by SU-MHGA

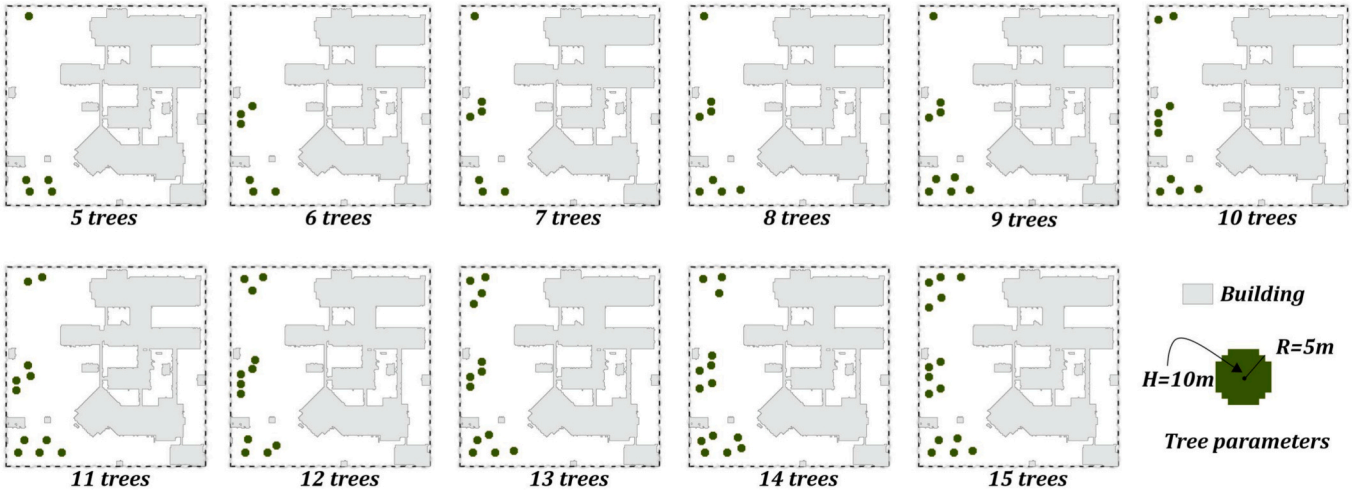

(b)Tree distribution obtained by TreePlanter

Fig. 27. Optimal tree locations by SU-MHGA and TreePlanter in Area C.

Appendix B. Influence of tree morphological parameters on optimized layouts

To evaluate the general applicability of the proposed framework under different design conditions, this study conducted supplementary experiments to analyze the influence of tree morphological parameters (size) on the optimized layouts and algorithmic performance. The three predefined tree types—short, tall, and large trees—were used for optimization with both SU-MHGA and TreePlanter in the same test area (Area A).

A comparison of computational performance demonstrates the exceptional stability of SU-MHGA. As shown in Fig. 28, regardless of changes in tree size, the optimization time for SU-MHGA remained consistently within the narrow range of 865 to 885 s. In contrast, the computational time for TreePlanter was highly sensitive to tree size, with its computational overhead increasing sharply, particularly when processing large trees, exceeding 30,000 s in some instances. This indicates that the computational complexity of SU-MHGA is minimally affected by variations in the physical parameters of the problem, endowing it with reliable efficiency for handling diverse real-world scenarios.

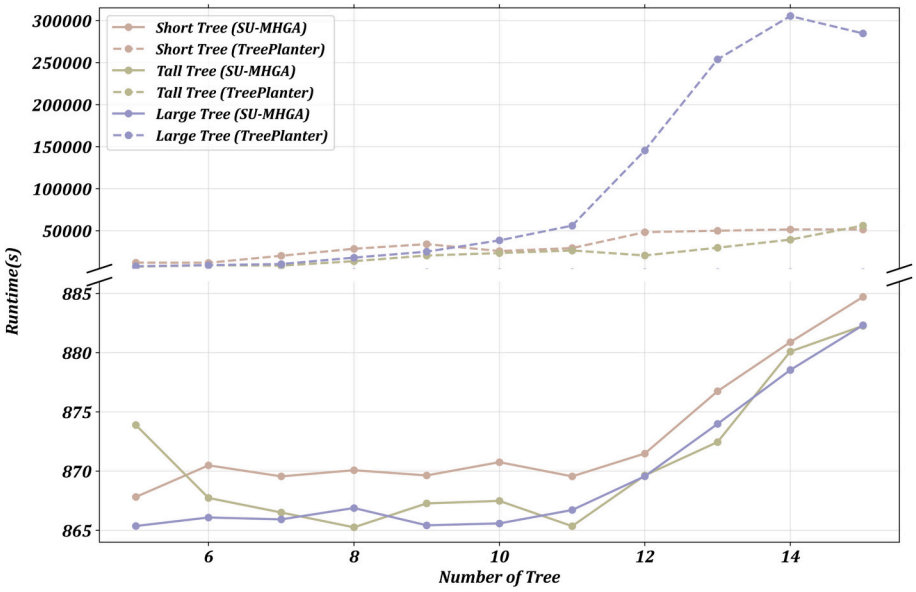

Fig. 28. Comparison of runtime optimization for three sizes of trees.

The comparison of cooling effectiveness and spatial layouts further confirms the superiority of SU-MHGA. As shown in Fig. 29, across all three tree sizes, the optimized layouts obtained by SU-MHGA resulted in lower $\overline{T_{mrt}}$ compared to those from TreePlanter, achieving superior cooling performance. Analysis of the spatial patterns of the optimized layouts (Figs. 30–32) reveals fundamental differences: TreePlanter tends to adopt relatively conservative and simplified layout strategies, whereas SU-MHGA can effectively explore a broader solution space, generating more complex and dispersed planting patterns. These patterns often involve strategically positioning trees near buildings to maximize shading on building facades and hardscapes, thereby more effectively mitigating the primary heat sources.

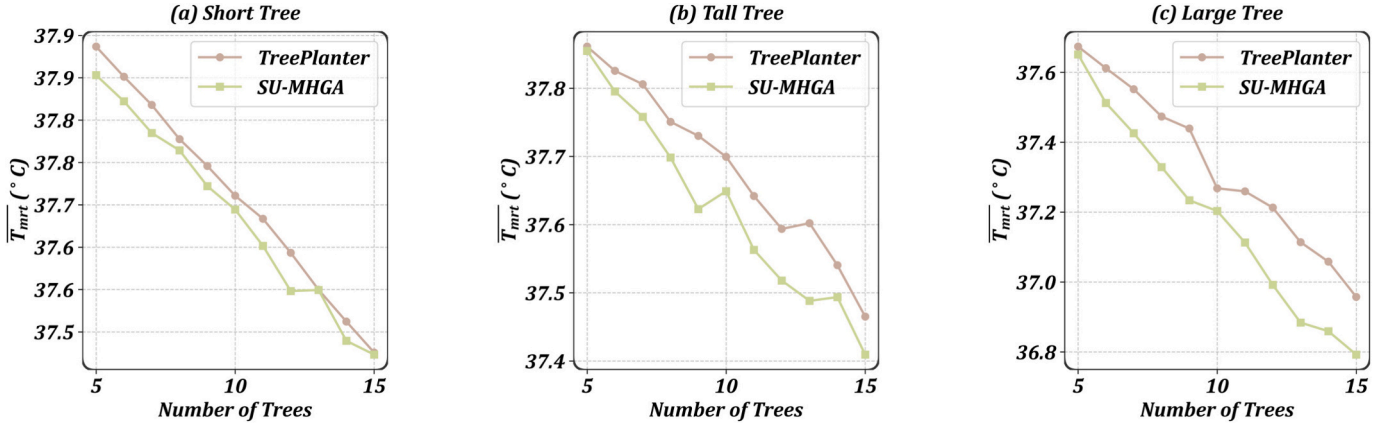

Fig. 29. Comparison of cooling effects for three sizes of trees.

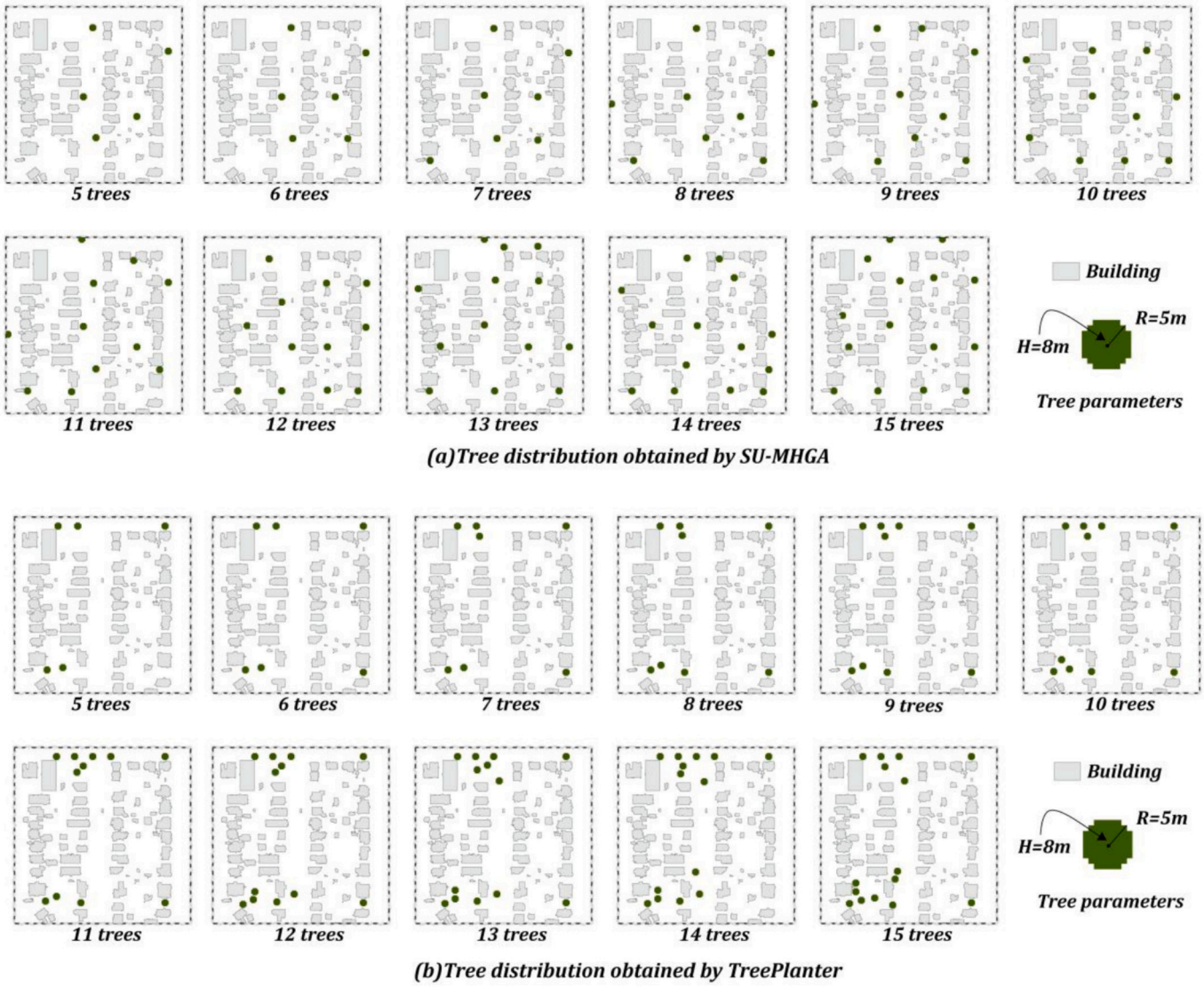

Fig. 30. Optimization results of SU-MHGA and TreePlanter for short trees.

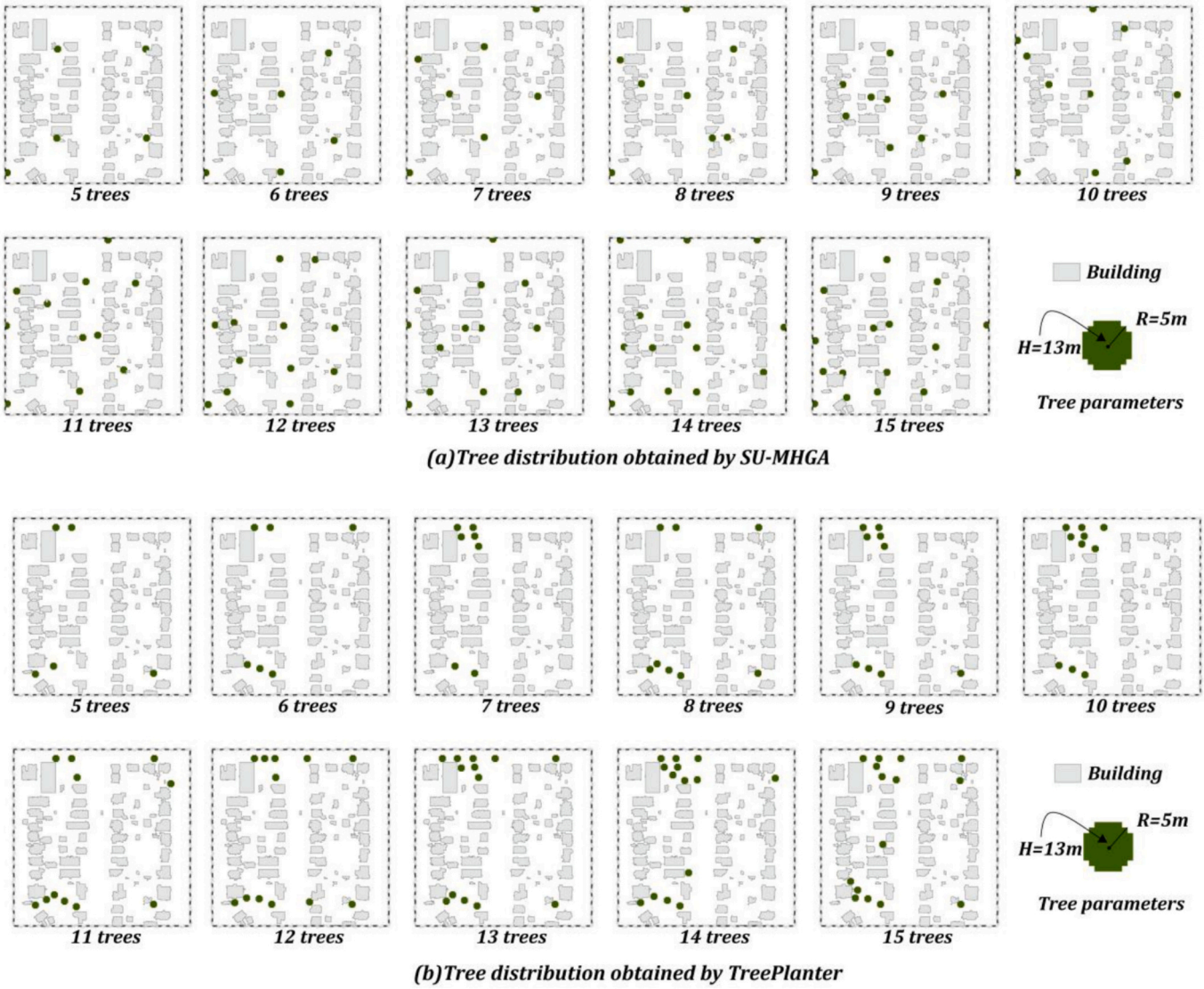

Fig. 31. Optimization results of SU-MHGA and TreePlanter for tall trees.

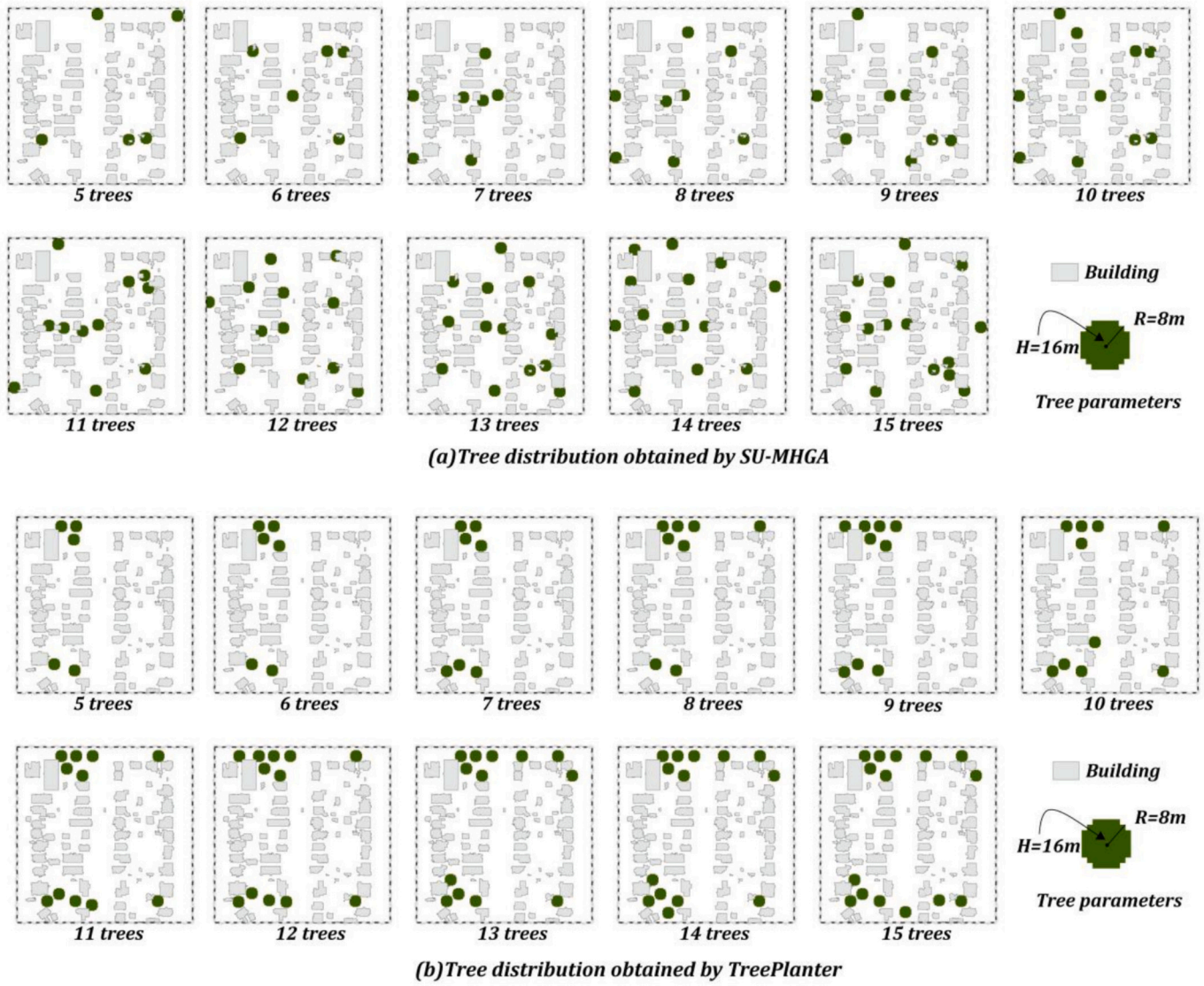

Fig. 32. Optimization results of SU-MHGA and TreePlanter for large trees.

In summary, the supplementary experiments indicate that the optimization performance of SU-MHGA—encompassing both computational efficiency and cooling effectiveness—is insensitive to variations in the predefined tree morphological parameters, demonstrating strong robustness. This enhances the general applicability of the framework in practical applications, as tree species and sizes in real-world planning are often diverse and predetermined.

Appendix C. Supplementary data

Supplementary data to this article can be found online at https://doi.org/10.1016/j.compenvurbsys.2026.102438.

Data availability

Data will be made available on request.

References

(USGS), U. S. G. S. (2023). *3D elevation program (3DEP) Lidar point cloud data: AZ PimaCo 2 2021*. OpenTopography.
Abdi, B., Hami, A., & Zarehaghi, D. (2020). Impact of small-scale tree planting patterns on outdoor cooling and thermal comfort. *Sustainable Cities and Society, 56*.
Abunnasr, Y., Mhawej, M., & Chrysoulakis, N. (2022). SEBU: A novel fully automated google earth engine surface energy balance model for urban areas. *Urban Climate, 44*.
Al-Ramadan, B., Aldosary, A. S., Kafy, A. A., Alsulamy, S., & Rahaman, Z. A. (2024). Unraveling the spatiotemporal dynamics of relative humidity in major saudi arabian cities: A synergy of climate modeling, regression analysis, and wavelet coherence. *Theoretical and Applied Climatology, 155*, 7909–7935.
An, L., Hang, J., Zhao, Y., Zeng, L., Dong, H., Zhao, Y., & Zhao, N. (2025). Cooling effects of tree transpiration: A CFD simulation study on heterogeneous tree canopy configurations (TCCs). *Sustainable Cities and Society, 126*.
Baño-Medina, J., Iturbide, M., Fernández, J., & Gutiérrez, J. M. (2024). Transferability and explainability of deep learning emulators for regional climate model projections: Perspectives for future applications. *Artificial Intelligence for the Earth Systems, 3*.
Baruti, M. M., Yahia, M. W., & Johansson, E. (2024). Spatial and temporal variations of microclimate and outdoor thermal comfort in informal settlements of warm humid Dar es Salaam, Tanzania. *Heliyon, 10*.
Bi, K., Xie, L., Zhang, H., Chen, X., Gu, X., & Tian, Q. (2023). Accurate medium-range global weather forecasting with 3D neural networks. *Nature, 619*, 533–538.

Bosch, M., Locatelli, M., Hamel, P., Remme, R. P., Jaligot, R., Chenal, J., & Joost, S. (2021). Evaluating urban greening scenarios for urban heat mitigation: A spatially explicit approach. *Royal Society Open Science, 8*.

Bowler, D. E., Buyung-Ali, L., Knight, T. M., & Pullin, A. S. (2010). Urban greening to cool towns and cities: A systematic review of the empirical evidence. *Landscape and Urban Planning, 97*, 147–155.

Briegel, F., Makansi, O., Brox, T., Matzarakis, A., & Christen, A. (2023). Modelling long-term thermal comfort conditions in urban environments using a deep convolutional encoder-decoder as a computational shortcut. *Urban Climate, 47*.

Cao, H., Wang, Y., Chen, J., Jiang, D., Zhang, X., Tian, Q., & Wang, M. (2022). Swin-Unet: Unet-like pure transformer for medical image segmentation. In *Proceedings of the IEEE/CVF Conference on Computer Vision and Pattern Recognition (CVPR)* (pp. 1–12).

Chen, H., Ooka, R., & Kato, S. (2008). Study on optimum design method for pleasant outdoor thermal environment using genetic algorithms (GA) and coupled simulation of convection, radiation and conduction. *Building and Environment, 43*, 18–30.

Chen, X., & He, B.-J. (2024). Planning for heat-resilient 15 min-cities: Opportunities, measurement, mechanism, and pathways. *Environmental Impact Assessment Review, 105*.

Church, R. L., & ReVelle, C. S. (1974). The maximal covering location problem. *Papers in Regional Science, 32*, 101–118.

Dennis, M., & James, P. (2016). Site-specific factors in the production of local urban ecosystem services: A case study of community-managed green space. *Ecosystem Services, 17*, 208–216.

Diallo, I., He, L., Koehler, K., Spira, A. P., Kale, R., Ou, J., … Augustinavicius, J. (2024). Community perspectives on heat and health in Baltimore city. *Urban Climate, 54*.

Du, J., Liu, L., Chen, X., & Liu, J. (2020). Field assessment of neighboring building and tree shading effects on the 3D radiant environment and human thermal comfort in summer within urban settlements in Northeast China. *Advances in Meteorology, 2020*, 1–19.

Elkhateeb, S., & Anwar, R. (2025). Parametric optimization of urban street tree placement: Computational workflow for dynamic shade provision in hot climates. *Urban Science, 9*.

Falk, T., Mai, D., Bensch, R., Çiçek, Ö., Abdulkadir, A., Marrakchi, Y., … Ronneberger, O. (2018). U-net: Deep learning for cell counting, detection, and morphometry. *Nature Methods, 16*, 67–70.

Froelich, N. J., Grimmond, C. S. B., & Schmid, H. P. (2011). Nocturnal cooling below a forest canopy: Model and evaluation. *Agricultural and Forest Meteorology, 151*, 957–968.

Ganjirad, M., Delavar, M. R., Bagheri, H., & Azizi, M. M. (2025). Optimizing urban critical green space development using machine learning. *Sustainable Cities and Society, 120*.

Gao, F., Lv, K., Jiang, Q.o., Xiao, H., & Li, J. (2025). How did the regional water-heat distribution in oasis area vary with the different spatial patterns and structures of shelterbelt system — A case study in Ulan Buh Desert oasis. *Agricultural and Forest Meteorology, 362*.

Ghasemi Tousi, E., O'Brien, W., Doulabian, S., & Shadmehri Toosi, A. (2021). Climate changes impact on stormwater infrastructure design in Tucson Arizona. *Sustainable Cities and Society, 72*.

Gkatsopoulos, P. (2017). A methodology for calculating cooling from vegetation evapotranspiration for use in urban space microclimate simulations. *Procedia Environmental Sciences, 38*, 477–484.

Grote, R., Samson, R., Alonso, R., Amorim, J. H., Cariñanos, P., Churkina, G., … Calfapietra, C. (2016). Functional traits of urban trees: Air pollution mitigation potential. *Frontiers in Ecology and the Environment, 14*, 543–550.

Hamed, M. M., Iqbal, Z., Nashwan, M. S., Kineber, A. F., & Shahid, S. (2023). Diminishing evapotranspiration paradox and its cause in the middle east and north africa. *Atmospheric Research, 289*.

Hao, T., Zhao, Q., & Huang, J. (2023). Optimization of tree locations to reduce human heat stress in an urban park. *Urban Forestry & Urban Greening, 86*.

Hein, S., & Spiecker, H. (2008). Crown and tree allometry of open-grown ash (*Fraxinus excelsior* l.) and sycamore (*Acer pseudoplatanus* l.). *Agroforestry Systems, 73*, 205–218.

Hosseinzadeh, A., & Keshmiri, A. (2021). Computational simulation of wind microclimate in complex urban models and mitigation using trees. *Buildings, 11*.

Hou, C. K. J., & Behdinan, K. (2022). Dimensionality reduction in surrogate modeling: A review of combined methods. *Data Science and Engineering, 7*, 402–427.

Jaluria, Y. (2009). Simulation-based optimization of thermal systems. *Applied Thermal Engineering, 29*, 1346–1355.

Jänicke, B., Milošević, D., & Manavvi, S. (2021). Review of user-friendly models to improve the urban Micro-climate. *Atmosphere, 12*.

Jiang, Y., Li, C., Li, X., Li, X., Song, T., & Liu, Y. (2024). Exploring the adaptive spatial patterns and impact factors for the cooling effect of park green spaces in riverfront area. *Urban Climate, 55*.

Kearl, Z., & Vogel, J. (2023). Urban extreme heat, climate change, and saving lives: Lessons from Washington state. *Urban Climate, 47*.

Keenan, O. J., Green, A. R., Young, A. R., Young, S. R., Katz, D. S. W., Miller, D. L., … Ghosh, A. K. (2025). Exploring community co-creation in tree planting and heat-related health interventions: A qualitative study. *International Journal of Environmental Research and Public Health, 22*.

Kim, J. Y., Park, C. Y., Lee, D. K., Yun, S. H., Hyun, J. H., & Kim, E. S. (2024). The cooling effect of trees in high-rise building complexes in relation to spatial distance from buildings. *Sustainable Cities and Society, 114*.

Kong, L., Lau, K. K.-L., Yuan, C., Chen, Y., Xu, Y., Ren, C., & Ng, E. (2017). Regulation of outdoor thermal comfort by trees in Hong Kong. *Sustainable Cities and Society, 31*, 12–25.

Lagerquist, R., Turner, D., Ebert-Uphoff, I., Stewart, J., & Hagerty, V. (2021). Using deep learning to emulate and accelerate a radiative-transfer model. *Journal of Atmospheric and Oceanic Technology, 38*, 1673–1696.

Li, Q., Fan, C., Xu, L., Luo, X., & Hu, M. (2025). Multi-modal ensemble deep learning model for microclimate prediction using urban morphological maps. *Energy, 337*.

Li, R., Zhao, Y., Chang, M., Zeng, F., Wu, Y., Wang, L., Niu, J., Shi, X., & Gao, N. (2024). Numerical simulation methods of tree effects on microclimate: A review. *Renewable and Sustainable Energy Reviews, 205*.

Lindberg, F., Grimmond, C. S. B., Gabey, A., Huang, B., Kent, C. W., Sun, T., … Zhang, Z. (2018). Urban multi-scale environmental predictor (UMEP): An integrated tool for city-based climate services. *Environmental Modelling & Software, 99*, 70–87.

Lindberg, F., Holmer, B., & Thorsson, S. (2008). SOLWEIG 1.0 – Modelling spatial variations of 3D radiant fluxes and mean radiant temperature in complex urban settings. *International Journal of Biometeorology, 52*, 697–713.

Liu, Z., Lin, Y., Cao, Y., Hu, H., Wei, Y., Zhang, Z., Lin, S., & Guo, B. (2021). Swin transformer: Hierarchical vision transformer using shifted windows. In *Proceedings of the IEEE/CVF International Conference on Computer Vision (ICCV)* (pp. 10012–10022).

Lu, D., & Ricciuto, D. (2019). Efficient surrogate modeling methods for large-scale earth system models based on machine-learning techniques. *Geoscientific Model Development, 12*, 1791–1807.

Lu, J., Kong, F., Yin, H., Middel, A., Kang, J., Wen, Z., & Liu, H. (2024). Evaluating sound attenuation of single trees using 3D information. *Journal of Environmental Management, 370*.

Lusk, A. C., da Silva Filho, D. F., & Dobbert, L. (2020). Pedestrian and cyclist preferences for tree locations by sidewalks and cycle tracks and associated benefits: Worldwide implications from a study in Boston, MA. *Cities, 106*.

Manickathan, L., Defraeye, T., Allegrini, J., Derome, D., & Carmeliet, J. (2018). Parametric study of the influence of environmental factors and tree properties on the transpirative cooling effect of trees. *Agricultural and Forest Meteorology, 248*, 259–274.

Matzarakis, A., & Rutz, F. (2007). Rayman: A tool for tourism and applied climatology. *Developments in Tourism Climatology*, 129–138.

Mayer, H., Holst, J., & Imbery, F. (2009). Human thermal comfort within urban structures in a central European city. In *The Seventh International Conference on Urban Climate*.

Mayer, H., & Höppe, P. (1987). Thermal comfort of man in different urban environments. *Theoretical and Applied Climatology, 38*, 43–49.

Meili, N., Manoli, G., Burlando, P., Carmeliet, J., Chow, W. T. L., Coutts, A. M., … Fatichi, S. (2021). Tree effects on urban microclimate: Diurnal, seasonal, and climatic temperature differences explained by separating radiation, evapotranspiration, and roughness effects. *Urban Forestry & Urban Greening, 58*.

Meshkova, V., Borysenko, O., Kucheryavenko, T., Vysotska, N., Skrylnyk, Y., Davydenko, K., & Holusa, J. (2024). Forest site and stand structure affecting the distribution of emerald ash borer, *Agrilus planipennis* fairmaire, 1888 (coleoptera: Buprestidae), in eastern Ukraine. *Forests, 15*.

Microsoft. (2021). *Swin-Tiny-Patch4-Window7-224*.

Morani, A., Nowak, D. J., Hirabayashi, S., & Calfapietra, C. (2011). How to select the best tree planting locations to enhance air pollution removal in the MillionTreesNYC initiative. *Environmental Pollution, 159*, 1040–1047.

Mu, W., & Li, C. (2024). Optimization of urban greenway route using a coverage maximization model for lines. *Computers, Environment and Urban Systems, 112*.

Nyelele, C., & Kroll, C. N. (2021). A multi-objective decision support framework to prioritize tree planting locations in urban areas. *Landscape and Urban Planning, 214*.

Ooka, R., Chen, H., & Kato, S. (2008). Study on optimum arrangement of trees for design of pleasant outdoor environment using multi-objective genetic algorithm and coupled simulation of convection, radiation and conduction. *Journal of Wind Engineering and Industrial Aerodynamics, 96*, 1733–1748.

Oswald, S. M., Revesz, M., Trimmel, H., Weihs, P., Zamini, S., Schneider, A., … Lindberg, F. (2019). Coupling of urban energy balance model with 3-D radiation model to derive human thermal (dis)comfort. *International Journal of Biometeorology, 63*, 711–722.

Pourreza, M., Moradi, F., Khosravi, M., Deljouei, A., & Vanderhoof, M. K. (2022). GCPs-free photogrammetry for estimating tree height and crown diameter in arizona cypress plantation using UAV-mounted GNSS RTK. *Forests, 13*.

Schneider, C., Neuwirth, B., Schneider, S., Balanzategui, D., Elsholz, S., Fenner, D., Meier, F., & Heinrich, I. (2021). Using the dendro-climatological signal of urban trees as a measure of urbanization and urban heat island. *Urban Ecosystems, 25*, 849–865.

Schuch, U. K. (2018). Tree irrigation requirements in the semiarid southwestern United States. *HortTechnology, 28*, 427–430.

Shaamala, A., & Yigitcanlar, T. (2024). Artificial intelligence in urban forestry: Strategic tree placement for improved climate adaptation. *Asia-Pacific Tech Monitor, 41*, 37–45.

Shlezinger, N., Eldar, Y. C., & Boyd, S. P. (2022). Model-based deep learning: On the intersection of deep learning and optimization. *IEEE Access, 10*, 115384–115398.

Stegmann, P. G., Johnson, B., Moradi, I., Karpowicz, B., & McCarty, W. (2022). A deep learning approach to fast radiative transfer. *Journal of Quantitative Spectroscopy and Radiative Transfer, 280*.

Stojakovic, V., Bajsanski, I., Savic, S., Milosevic, D., & Tepavcevic, B. (2020). The influence of changing location of trees in urban green spaces on insolation mitigation. *Urban Forestry & Urban Greening, 53*.

Strohbach, M. W., Lerman, S. B., & Warren, P. S. (2013). Are small greening areas enhancing bird diversity? Insights from community-driven greening projects in Boston. *Landscape and Urban Planning, 114*, 69–79.

Tan, C. L., Wong, N. H., & Jusuf, S. K. (2013). Outdoor mean radiant temperature estimation in the tropical urban environment. *Building and Environment, 64*, 118–129.
Tan, Z., Lau, K. K.-L., & Ng, E. (2017). Planning strategies for roadside tree planting and outdoor comfort enhancement in subtropical high-density urban areas. *Building and Environment, 120*, 93–109.
Tang, J., Zhao, Z., Guo, Y., Wang, C., Zhang, X., Yan, R., & Chen, X. (2024). Privacy-preserving federated transfer learning for defect identification from highly imbalanced image data in additive manufacturing. *Robotics and Computer-Integrated Manufacturing, 89*.
Thorsson, S., Rocklöv, J., Konarska, J., Lindberg, F., Holmer, B., Dousset, B., & Rayner, D. (2014). Mean radiant temperature – A predictor of heat related mortality. *Urban Climate, 10*, 332–345.
Toparlar, Y., Blocken, B., Maiheu, B., & van Heijst, G. J. F. (2017). A review on the CFD analysis of urban microclimate. *Renewable and Sustainable Energy Reviews, 80*, 1613–1640.
Wallenberg, N., Lindberg, F., & Rayner, D. (2022). Locating trees to mitigate outdoor radiant load of humans in urban areas using a metaheuristic hill-climbing algorithm – Introducing TreePlanter v1.0. *Geoscientific Model Development, 15*, 1107–1128.
Wang, C., Wang, Z.-H., & Ryu, Y.-H. (2021). A single-layer urban canopy model with transmissive radiation exchange between trees and street canyons. *Building and Environment, 191*.
Wang, J., Zhou, W., & Jiao, M. (2022). Location matters: Planting urban trees in the right places improves cooling. *Frontiers in Ecology and the Environment, 20*, 147–151.
Wang, Y., Wang, J., Zhang, H., & Song, J. (2025). Bridging prediction and decision: Advances and challenges in data-driven optimization. *Nexus, 2*.
Wang, Z., Li, Y., Song, J., Wang, K., Xie, J., Chan, P. W., … Di Sabatino, S. (2022). Modelling and optimizing tree planning for urban climate in a subtropical high-density city. *Urban Climate, 43*.
Watson, C., Cooper, N., Palacio, D. N., Moran, K., & Poshyvanyk, D. (2022). A systematic literature review on the use of deep learning in software engineering research. *ACM Transactions on Software Engineering and Methodology, 31*, 1–58.
Wolpert, D. H., & Macready, W. G. (1997). No free lunch theorems for optimization. *IEEE Transactions on Evolutionary Computation, 1*, 67–78.
Wu, R., Wu, N., Nan, X., Yan, H., Wang, K., Ma, T., … Bao, Z. (2023). Effects of the bamboo communities on microclimate and thermal comfort in subtropical climates. *Forests, 14*.
Wu, Y., Zhan, Q., Quan, S. J., Fan, Y., & Yang, Y. (2021). A surrogate-assisted optimization framework for microclimate-sensitive urban design practice. *Building and Environment, 195*.
Wu, Z., & Chen, L. (2017). Optimizing the spatial arrangement of trees in residential neighborhoods for better cooling effects: Integrating modeling with in-situ measurements. *Landscape and Urban Planning, 167*, 463–472.
Wu, Z., Dou, P., & Chen, L. (2019). Comparative and combinative cooling effects of different spatial arrangements of buildings and trees on microclimate. *Sustainable Cities and Society, 51*.
Xie, H., Wang, C., Zhao, J., Liu, Y., Dan, J., Fu, C., & Sun, B. (2024). PRCL: Probabilistic representation contrastive learning for semi-supervised semantic segmentation. *International Journal of Computer Vision, 132*, 4343–4361.
Xu, H., Wang, C. C., Shen, X., Zlatanova, S., & Paolini, R. (2025). Refined definition of level-of-detail for tree models in support of microclimate simulation. *Sustainable Cities and Society, 126*.
Xu, Y., Vahmani, P., Jones, A., & Hong, T. (2024). Anthropogenic heat from buildings in los Angeles county: A simulation framework and assessment. *Sustainable Cities and Society, 107*.
Yun, S. H., Lee, D. K., Piao, Z. G., Park, C. Y., Kim, S. H., & Kim, E. S. (2023). Developing a three-dimensional urban surface model for spatiotemporal analysis of thermal comfort with respect to street direction. *Sustainable Cities and Society, 97*.
Zani, M., Panettieri, E., & Montemurro, M. (2024). Optimisation of interlayer temperature in wire-arc additive manufacturing process using NURBS-based metamodel. *International Journal of Material Forming, 17*.
Zhang, T., Spence, C., Qi, F., Yang, W., & Song, T. (2022). Influence of tree location on thermal radiation disturbance of the west wall of summer buildings. *Energy and Buildings, 273*.
Zhang, X., Wang, Y., Zhou, D., Yang, C., An, H., & Teng, T. (2022). Comparison of summer outdoor thermal environment optimization strategies in different residential districts in Xian, China. *Buildings, 12*.
Zhang, Y., Long, M., Chen, K., Xing, L., Jin, R., Jordan, M. I., & Wang, J. (2023). Skilful nowcasting of extreme precipitation with NowcastNet. *Nature, 619*, 526–532.
Zhao, Q., Sailor, D. J., & Wentz, E. A. (2018). Impact of tree locations and arrangements on outdoor microclimates and human thermal comfort in an urban residential environment. *Urban Forestry & Urban Greening, 32*, 81–91.
Zhao, Q., Wentz, E. A., & Murray, A. T. (2017). Tree shade coverage optimization in an urban residential environment. *Building and Environment, 115*, 269–280.
Zhao, Z., Li, H., & Wang, S. (2024). Machine learning-based surrogate models for fast impact assessment of a new building on urban local microclimate at design stage. *Building and Environment, 266*.
Zheng, S., Guldmann, J.-M., Wang, Z., Qiu, Z., He, C., & Wang, K. (2021). Experimental and theoretical study of urban tree instantaneous and hourly transpiration rates and their cooling effect in hot and humid area. *Sustainable Cities and Society, 68*.
Zheng, Y., Ren, C., Shi, Y., Yim, S. H. L., Lai, D. Y. F., Xu, Y., … Li, W. (2023). Mapping the spatial distribution of nocturnal urban heat island based on local climate zone framework. *Building and Environment, 234*.